ENHANCING SOLAR PHOTOVOLTAIC EFFICIENCY WITH POROUS SILICA COATINGS

A THESIS SUBMITTED IN PARTIAL FULFILLMENT OF THE

REQUIREMENTS FOR THE DEGREE OF

MASTER OF SCIENCE IN RENEWABLE ENERGY

OF

THE UNIVERSITY OF NAMIBIA

BY

LEONARD ETUNA NAMWIHA

222177225

APRIL 2025

MAIN SUPERVISOR: DR. PETJA DOBREVA (UNIVERSITY OF NAMIBIA)

CO-SUPERVISORS:

PROF. DR. BRYCE S. RICHARDS (KARLSRUHE INSTITUE OF TECHNOLOGY)

AND

DR GAN HUANG (KARLSRUHE INSTITUE OF TECHNOLOGY)

Abstract

Solar surface glass is known to exhibit reflectance loss of no less than 4%, depending on the angle of the incident light. Furthermore, the high operating temperature of the solar photovoltaic (PV) module also reduces the solar PV module efficiency by approximately $0.45 - 0.50\ \%/℃$ depending on the temperature coefficient and the type of the solar modules[1]. The study investigated porous silica which is known to have high transmittance in the solar spectrum range (0.3-1.1μm) and high emissivity in the mid-infrared range (8-13μm) due to its bonding structure. The research employed the base/acid double catalysis technique of the sol-gel method, using Pluronic F127 as a surfactant, Tetraethylorthoxysilicate (TEOS), ethanol, hydrochloric acid, ammonium hydroxide, hexamethyldisilazane (HMDS) and distilled water to synthesise silicon dioxide sol. The sol was afterwards spin-coated on a glass substrate, resulting in a porous silica layer approximately 200 nm thick. Scanning Electron Microscopy (SEM), Fourier Transform Infrared Spectroscopy (FTIR), and Ultraviolet-Visible-Near Infrared Spectroscopy (UV-Vis-NIR) spectrophotometer were employed to investigate the optical characteristics of the coatings. The study achieved an approximate 2% increase in transmittance within the solar spectrum (0.3-1.1μm) with a single porous silica layer with 8% emissivity in the mid-infrared range (8-13μm). In addition, it observed a nearly 20% enhancement in emissivity with three layers in the mid-infrared range (8-13μm), while transmittance in the solar spectrum (0.3-1.1μm) decreased almost linearly by 8% from 0.3-0.55μm with three layers.

Keywords: Porous silica, sol-gel method, anti-reflective coating, radiative cooling, transmittance, emissivity

List of Conference Proceedings

- Namwiha, L.E. (2024) Enhancing solar photovoltaics efficiency with porous silica coatings. Proceedings of the Jcol Youth for Green Hydrogen (YAH2) Scholarship Programme Visibility Event – Germany and Namibia Partnership. Berlin, Germany.

Table of Contents

List of Tables

List of Figures

List of Abbreviations and Acronyms

AR – Anti-reflective

ARC – Anti-reflective coatings

CVD - Chemical Vapor Deposition

EVA - Ethylene Vinyl Acetate copolymer

FTIR - Fourier Transform Infrared Spectroscopy

GRIN - Graded Refractive Index

HMDS - Hexamethyldisilane

PF127 – Pluronic F127

PV - Photovoltaics

PVD - Physical Vapor Deposition

PVF- Polyvinyl Fluoride

RPECVD - Remote plasma-enhanced chemical vapour deposition

SEM - Scanning Electron Microscopy

Si $(OC_2H_5)_4$ - Tetraethyl orthosilicate

Si-O-Si - Siloxane bonds

Si-OH - Silanol groups

TEM - Transmission Electron Microscopy

TEOS – Tetraethyl orthosilicate

UV-Vis-NIR - Ultraviolet-Visible-Near Infrared Spectrophotometer

Acknowledgements

I am deeply appreciative of the following individuals and organisations:
Dr. Petja Dobreva, I am grateful for your unwavering support, patience, and leadership during my research. Your dedication, expertise, and knowledge in the field of renewable energy, notably PV technology, were greatly treasured and invaluable. I will always be grateful for the chance you gave me to conclude my postgraduate studies in renewable energy.
Prof. Bryce Richards, I am grateful for the privilege of conducting my research at the Institute of Microstructure Technology (IMT) at the Karlsruhe Institute of Technology and for the valuable expertise and for helping me to complete this study.
Dr. Gan Huang, I am extremely grateful for your unwavering support and dedication to guaranteeing that I have all the necessary resources to complete this research project. Thanks to your constant motivation, I have obtained great research skills from engaging with you.
Dr. Markus Guttmann, I am grateful for the opportunity to utilise the laboratories in your department at IMT for my chemical processes. I am extremely grateful for the safety training you provided and all the necessary support I needed.
To Mr. Ehrhardt Marco and Ms. Xinyun Zhang for offering me the necessary support and training with laboratory equipment. Furthermore, thanks to the Karlsruhe Institute of Technology (KIT) and Institute of Microstructure Technology (IMT), the Southern African Science Service Centre for Climate Change and Adaptive Land Management (SASSCAL), The Federal Ministry of Education and Research (BMBF) and the University of Namibia (UNAM) for making this study possible.

Dedications

This study is dedicated to my mother Mrs. Esther Amukoto.

"There is plenty of room at the bottom" – Richard Feynman

Declarations

I, Leonard Etuna Namwiha, hereby declare that this study is my own work and is a true reflection of my research and that this work, or any part thereof has not been submitted for a degree at any other institution.

Leonard Etuna Namwiha		April 2025
Name of Student	**Signature**	**Date**

Chapter 1

Introduction

This chapter provides a context for this study and explains the problem to be solved as well as the study's significances, goals and objectives.

1.1 Background of the study

There is a growing demand for improvement of solar photovoltaic (PV) efficiency as factors that affect their efficiency have led to a reduction in energy output[2], [3]. Some of the losses that are experienced by the solar modules are caused by reflection losses and high operating temperatures[4], [5]. It is known that at the interface of the PV module glass surface and air, there is a reflection loss of no less than 4% of the incident light, depending on the angle of incidence [6]. The high reflection losses result in less light reaching the solar cells for the generation of electron-hole pairs, which reduces the amount of power generated by the solar cells[7]. High temperature also leads to a reduction in the output voltage[8], [9]. Furthermore, it is known that for every 1°C rise in temperature above 25°C, the panel's maximum power output decreases by 0.45-0.50%/℃ [10]. This reduction in efficiency is due to the narrowing of the semiconductor bandgap at higher temperatures, which decreases voltage output and overall efficiency.

Optical coatings on the PV panel's glass offer a practical approach to reducing reflective losses and increasing the panel's efficiency [9]. Important parameters of an anti-reflective (AR) coating are its refractive index (n_c) and its thickness (d_c). The

thickness d_c of the coating should be: $d_c = \frac{\lambda}{4n_c}$, where lambda ($\lambda$) is the wavelength of the incident light and n_c[11]. In most cases, the thickness of the AR coating is less than 200 nm, and it is preferred in solar PV surfaces, depending on the desired solar spectrum wavelength range[12], [13], [14]. The AR coatings on the solar module glass surface should allow light transmission within the range of 300-1100 nm of the solar spectrum[6]. However, there is a further need for a durable AR coating with high thermal, chemical, and mechanical properties.

Porous silica is one of the most promising AR coatings known today[6]. Porous silica is known for its low reflective index, and lower density of about 1.4 g/cm^3 and ability to dissipate heat, which may aid in the cooling of solar modules[15]. Studies have shown how with porosity, a refractive index of porous silica can be reduced from 1.46 to 1.23 with the nanoporous silica particle size between 12-13nm [16]. Porous silica coatings' porosities and sizes of nanoparticles can be tuned depending on the preferred coating and can be made to withstand humidity, soiling, and high-temperature environments[17], [18], [19].

Although studies focused on fabricating silica with different porosity to reduce the reflective index and increase transmittance, none of the studies so far have focused on fabricating porous silica coatings with different porosity to measure their radiative cooling on a solar module surface. The only study that have been observed to involve combining silica in radiative cooling and AR coating for solar PV, simply focused on radiative selective coating layer, a combination of SiO_2, Al_2O_3, SiN_4 and TiO_2,

although achieving 1.9℃ reduction in operating temperature, it was observed to be difficult to commercialise[20].

Porous silica coatings with optimized pore size and porosity will reduce reflection losses and improve radiative cooling, enhancing PV efficiency. This study focuses on fabricating porous silica with different pore sizes and porosities to assess its radiative cooling properties and how it can be used in reducing the operating temperature of the photovoltaic module to enhancing its efficiency. The study seeks to address how the variations in pore sizes and porosities of porous silica coatings affect the reflectance, transmittance and emissivity of solar PV modules. This study is of great significance to real-world solar PV industries as it helps the PV manufacturer to fabricate more efficient PV modules for the world renewable energy transition[21]. It is also important to PV system owners as it allows their PV systems to harness more energy from the sun even under high temperatures.

1.2 Problem Statement

The pore sizes and porosities of porous silica coatings can significantly affect the light transmittance, heat dissipating properties, and durability of the coatings, but these effects were not investigated sufficiently.

1.3 Aims and Objectives

- To fabricate porous silica coatings with varying pore sizes and porosities.
- This work focuses on fabricating porous silica coatings with optimum radiative cooling properties to enhance the efficiency of solar PV.
- To characterise transmittance, reflectance, thermal emissivity, and wettability of the fabricated coating.
- To assess the hydrophobicity and mechanical properties of the fabricated coatings.

This thesis is organised in the following way:

Chapter 2 offers a literature review on porous silica coatings and radioactive cooling for solar PV.

Chapter 3 focuses on the research method used in this study to fabricate porous silica coatings,

Chapter 4 presents the results and discussions for the fabricated porous silica coatings, while,

Chapter 5 provides the conclusions and recommendations of this study.

Chapter 2

Literature Review

This chapter gives a review of the solar photovoltaic basic principles, AR coatings, sol-gel methods, methods of AR coating depositions, porous silica and the combination of porous silica as an AR coating and passive radiative cooling for enhancing solar PV efficiency.

2.1 Light reflection and temperature effects on solar PV output

Solar radiation is directly converted into usable energy using solar PV systems. The fundamental component of a photovoltaic system is the photovoltaic cell, a semiconductor device that transforms solar radiation into direct-current electricity[22]. Usually ranging from 50 to 200W, a PV module is composed of interconnected PV cells[23]. A PV system is made up of PV modules together with a few more specific system parts such as batteries, inverters, electrical parts, and mounting systems[24].

Monocrystalline panels are recognised as the most efficient type existing commercially, with efficiency ratings typically ranging from 18% to 22% under standard test conditions[25], [26]. The monocrystalline temperature coefficient typically ranges from -0.3%/°C to -0.5%/°C[26]. This means that for every degree Celsius increase in temperature, monocrystalline panels lose about 0.3%/℃ to 0.5%/℃ of their power.

The solar panel itself is covered by a low-iron glass that allows more light to be transmitted through it[27]. Many solar surface glasses are investigated to have the transmittance altered around 90%[27].

2.1.1. Reflection and scattering of light

When light passes from one medium to another is known as refraction, while when light is reflected then it is known as reflection. The reflected light depends on many factors like wavelength, surface roughness and surface refractive index[28].

Rayleigh and Mie Scatterings are some of the scattering phenomena experienced by electromagnetic light waves when interacting with particles of various sizes[29]. Rayleigh scattering is elastic scattering that occurs when light interacts with particles much smaller than its wavelength, typically less than 1/10th of the wavelength[28]. Rayleigh scattering is highly wavelength-dependent, with shorter wavelengths scattered more effectively than longer ones.
The scattering of light by nanoparticles is governed by Rayleigh scattering principles. According to Rayleigh's theory, when light interacts with particles much smaller than its wavelength, the intensity of scattered light is inversely proportional to the fourth power of the wavelength (λ^{-4}). This means shorter wavelengths are scattered more effectively than longer wavelengths. In terms of particle sizes, smaller particles (2-50 nm) scatter light of shorter wavelengths less aggressively, allowing for better transmission of visible light while reducing glare and reflections. This is crucial in applications like anti-reflective coatings where clarity and visibility are essential. While larger particles (>50 nm) tend to scatter more light overall, which can lead to increased reflection and reduced effectiveness of the coating[29], [30].

2.1.2. Radiative cooling

Radiative cooling is a natural process by which an object loses heat by emitting thermal radiation. It occurs when an object emits more radiation than it absorbs, leading to a net loss of heat energy[31], [32].

Radiative cooling works by allowing an object to emit infrared radiation, particularly through the atmospheric transparency window (8–13 μm), where the Earth's atmosphere is most transparent to thermal radiation[9], [33]. This allows heat to be radiated away into outer space, which is at a much lower temperature than the Earth's surface.

Implementing radiative cooling effectively can be challenging due to the need for specialized materials with high emissivity in the infrared range. Environmental factors such as humidity, cloud cover, and wind speed can also affect performance[2], [34]. Furthermore, the radiative cooling coating is applied to solar surface glass to enhance the cooling efficiency of solar modules by dissipating excess heat through the emission of infrared radiation as shown in Figure 3[20], [35].

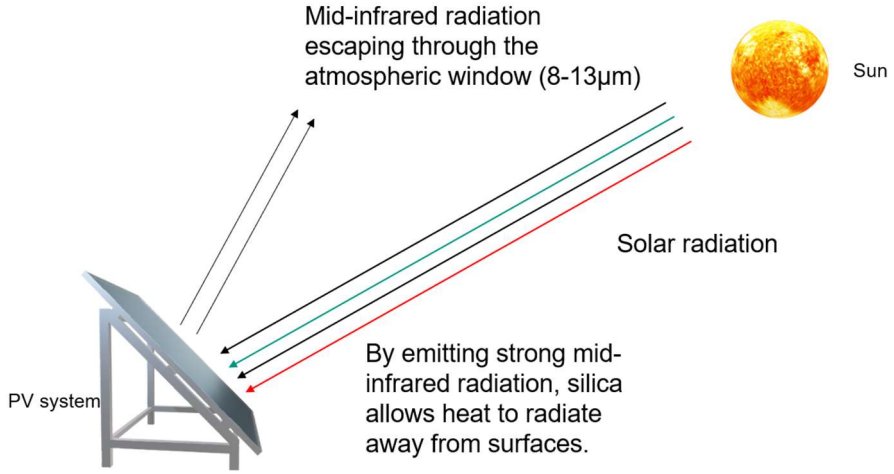

Figure 1 A schematic view of a solar photovoltaic module that emits mid-infrared radiation

A hexagonal array of photonic silica microcylinders can be etched into the top surface of solar module glass. These structures enhance passive radiative cooling by increasing the mid-infrared radiation emissivity of the glass. The microcylinders cause multipolar Mie-like resonances, which lead to antireflection effects in the infrared spectrum. This design improves the average emissivity from 84.3% to 97.7% in the 7.5–16 μm wavelength range, which is crucial for effective cooling, while maintaining transparency for visible light in the 300-1100 nm solar spectrum range[35].

Silica nanoshells embedded in a polymer matrix can also be used for daytime radiative cooling. These nanoshells provide a strong diffuse reflection of sunlight, minimizing solar absorption while allowing selective thermal radiation. This approach helps achieve sub-ambient temperatures without a glaring reflective surface, making it suitable for practical applications.

Multipolar Mie-like resonances in dielectric structures, such as a hexagonal array of silica microcylinders, enhance infrared emissivity. The ability to design and manipulate these resonances provides flexibility in creating materials with tailored optical properties. This is particularly useful in engineering dielectric meta-structures that maximize cooling efficiency while maintaining other desired optical characteristics.

Passive radiative cooling constitutes an emerging and sustainable approach to inducing a cooling effect without reliance on electricity or any other external energy input. It is noticed that for radiative cooling to take place, it is required that above 97% reflection in the solar spectrum (0.25–2.5 μm) and maximum emission in the atmospheric window (8–13 μm). However, for solar PV the need is to achieve maximum anti-reflection of light in the solar band and emission in the thermal band for passive radiative cooling to take place[36]. Radiative cooling takes place when there is a

difference in temperature between the materials, leading to a transfer of heat from the hotter medium to a colder medium through convection, conduction, and radiation. According to this equation 1 on passive radiative cooling (PRC), the net cooling power P_{net} can be expressed as[37]:

$$\mathrm{P_{net}(T) = P_{rad}(T) - P_{atm}(T_{atm}) - P_{solar} - P_{cond+convect}} \quad (1)$$

Where, T represents the surface temperature of the cooler and T_{atm} represents the ambient temperature. P_{rad} shows the outward heat radiation of the cooler surface, P_{solar} is for the radiation absorbed by the sun, P_{atm} represents the thermal radiation absorbed from the atmosphere, and $P_{cond+conv}$ represents conduction and convection, the non-radiative heat between the cooler and the surrounding environment.

In the photovoltaic module, the temperature of the solar module increases with the increase in the ambient temperature, this leads to the increase in the operating temperature of the solar module. In contrast, the increase in the operating temperature beyond the standard temperature of 25℃ of the solar module leads to decreased efficiency of the solar module. The solar module is made up of polyvinyl fluoride PVF (tedlar), ethylene vinyl acetate copolymer (EVA) and a top glass tolar cell followed by a strong back sheet[38], [39].

When the temperature increases it is known that it is difficult to evacuate heat from the solar module where there is a temperature difference of 2℃ between EVA and solar cells, and 3℃ between the EVA and the interface glass [40]. Porous silica coating is known as radiative cooling and anti-reflective coating, and the combination of both

may assist in evacuating heat from the module and in preventing excess heat from building up within the solar photovoltaic. Radiative cooling of the coating depends on the thickness of the coating and the porosity of the coating. Porous silica coatings exhibit high radiative emissivity in the atmospheric transparency window (8-13 μm) compared to other materials, making them attractive for passive radiative cooling applications.

2.2 Anti-Reflective Coatings

Reflection loss is one of the factors that lead to lower efficiency of the solar modules. There has been a growing demand to develop anti-reflective coatings at the interface of the solar glass surface and the air to minimise this reflection loss. Given their ability to minimise light reflection and improve transmission through surfaces, ARCs, are crucial for some optical applications, such as lenses, solar cells, and camera optics, in addition to solar PV panels.

The anti-reflective coating used in solar PV panels needs to have certain properties like a refractive index between that of the air (which is 1) and that of the glass which is approximately 1.52. This means the ideal refractive index of the coating should be 1.23, which is obtained by equation 2.

$$n_{ideal} = \sqrt{n_{air} n_{glass}}\,, \qquad (2)$$

The coating should have high transmittance in the solar spectrum range of 300 nm-1100 nm (for modules made of silicon solar cells). To obtain the suitable thickness the following formula (3) is utilised, d is for the thickness and λ represent the wavelength of light transmitted.

$$d = \frac{4}{\lambda} \qquad (3)$$

Many anti-reflective coatings have been developed, although they differ in efficiency, chemical resistance, durability, and in terms of their soiling and wettability properties.

Only one material in nature has a refractive index close to the ideal 1.23, this is MgF_2 with a refractive index of 1.38. However, different elements and compounds can be combined to achieve the ideal refractive index required for anti-reflective coatings of the top glass surface of the solar module. Various elements or compounds have been combined to develop anti-reflective coatings for applications in optics and medical imaging. In the solar photovoltaic industry, ARC layers of different compounds are applied on a glass surface or solar cells and are properly designed to minimise reflection loss of desirable light and increase the maximum power output of the solar PV panel.

Magnesium Fluoride (MgF_2) has been used in AR coatings, and it is known to have a refractive index of approximately 1.38. It is known to be effective as a single-layer coating, reducing reflection from about 4% to approximately 1% at 300-1100nm wavelengths. Offers good durability and mild abrasion resistance, but care is needed during cleaning to avoid damage[41].

Apart from magnesium fluoride, silicon Nitride (Si_3N_4), having a refractive Index typically around 2.0, it provides good anti-reflective performance too, especially in the near-infrared region[42]. It can be deposited using plasma-enhanced chemical vapour deposition (PECVD) for improved durability.

Titanium Dioxide (TiO_2) with a refractive Index of about 2.4, its high refractive index allows it to be effective in reducing reflections when layered with lower-index materials. Often used in conjunction with other materials to achieve optimal performance[43].

Furthermore, more Silicon Dioxide (SiO_2) has a refractive index of approximately 1.46. it is known for its hardness and scratch resistance, making it suitable for durable applications[44]. Zirconium Dioxide (ZrO_2) has a refractive index of about 2.1, It provides high durability and can be effective when layered with lower-index materials to optimize reflectance[45].

In addition, Aluminium Oxide (Al_2O_3) and Zinc Oxide (ZnO) are also used in AR coatings. Aluminium Oxide has a refractive index typically around 1.76, it can achieve broadband performance through structural modifications, and durability against wear and laser damage[43]. Zinc Oxide (ZnO): The refractive index of zinc oxide typically ranges from 1.85 to 1.91 in the visible spectrum, which allows it to effectively reduce reflections when layered appropriately with other materials[43], [46].

Zinc oxide serves as an effective anti-reflective coating due to its favourable refractive index, low reflection characteristics, excellent UV-blocking capabilities, and durability. Its application across various fields highlights its versatility and effectiveness in enhancing optical performance while protecting sensitive materials from UV damage[46].

Although some compounds used in anti-reflective coatings may appear to have high reflective index, they can be synthesised or mixed with other elements in such that it lowers their reflective index. Some templating agents can also be included in the

coatings to make them more porous, the nanopores can be used to introduce in the coatings small air spaces as these spaces allows solar radiations to be easily transmitted through, this is because air has a lower refractive index and the combination of air or empty nanopores leads to a reduction in the refractive index.

Antireflection coatings (ARCs) are primarily employed to mitigate Fresnel reflection losses during light transmission between different mediums. There are two primary strategies to attain the antireflection effect: one involves the deposition of thin films, including single, double, and multi-layer films on the substrate, while the other employs graded refractive index (GRIN) coatings utilising porous and nanostructured arrays, such as moth-eye structures.

There are various processes and techniques to syntheses nanostructured coatings which include thermal evaporation, magnetron sputtering, and sol-gel techniques. Each method offers different advantages regarding control over film thickness, uniformity, and scalability. Furthermore, advanced deposition techniques like Dynamic Glancing Angle Deposition (DGLAD) have been employed to enhance wear resistance and mechanical properties of the coatings while maintaining their optical performance[47]. The effectiveness of GRIN coatings is often evaluated based on their reflectance and transmittance characteristics across specific wavelength ranges[44]. Additionally, optimizing parameters such as film thickness and porosity through careful control during fabrication can lead to significant improvements in optical performance. should also satisfy the thickness of $d = \frac{4}{\lambda}$ and following the Fresnel law of reflection.

These GRIN coatings utilise a gradient in refractive index, which can be achieved through various methods, including the incorporation of porous and nanostructured materials.

Porous silica layers can be fabricated using sol-gel processes or remote plasma-enhanced chemical vapor deposition (RPECVD). These methods allow for the control of porosity and thickness, crucial for optimizing the refractive index profile.

The integration of nanoparticles into the coating matrix can further enhance the performance of GRIN coatings. By manipulating the size and distribution of nanoparticles, tailored refractive indices can be achieved.

A notable approach involves using polystyrene (PS) as a template to create voids within silica nanoparticle films, resulting in a significant drop in refractive index due to increased porosity[48]. This technique allows for the creation of highly porous networks that maintain mechanical integrity while achieving low reflectance.

Biomimetic designs inspired by natural structures, such as moth eyes or leaf surfaces, have shown promise in creating effective antireflective coatings. These structures can facilitate light trapping and reduce reflection over broad wavelength ranges. For example, nanostructured surfaces that mimic the hierarchical organization found in nature have been developed to achieve both antireflective properties and self-cleaning functionalities.

Anti-reflective coatings are commonly designed with nanoparticles ranging from 2 nm -100 nm in size in diameter, with most common nanoparticles' size ranging between 10 nm -50 nm[49]. The size of nanoparticles matters in minimising the scattering of lights and reflection of lights of different wavelengths with bigger particles scattering more lights and smaller particles scattering lights of shorter wavelengths, utilising the

light scattering principles[50]. Furthermore, with anti-reflective coatings it is possible to achieve a 99.4 transmittance in the solar spectrum like visible light range[51].

2.3. Sol-Gel Method

Sol-Gel is a versatile method for synthesising materials, particularly metal oxides, through the hydrolysis and condensation of metal alkoxides. Applications such as coatings, ceramics, and nanomaterials widely employ this technique[52].

The Sol-Gel process involves two crucial steps: hydrolysis, which involves mixing metal alkoxides with water. The alkoxide groups react with water to form hydroxyl groups and alcohol[53]. This step leads to the formation of a sol, a colloidal suspension of nanoparticles[52]. The second step is condensation, where the hydroxyl groups undergo reactions to form bonds between particles[54], [55], [56]. This process results in the growth of nanoparticles and can lead to the formation of a gel network. The gel transitions from a liquid-like sol to a solid-like gel as the particles aggregate.

The sol-gel process is widely used for coatings as it provides excellent adhesion, durability, and resistance to corrosion[57]. The production of advanced ceramics with tailored properties for structural and functional applications utilises sol-gel. Sol-gel also contributes to the development of thin films for optical coatings and sensors.

The advantages of the sol-gel process are that it allows for precise control over the chemical composition and microstructure of the final product. Low processing temperatures enable the production of a wide range of materials such as glasses, ceramics, and thin films. Furthermore, the ability to produce nanoparticles enables its applications in catalysis, electronics, and biomedicine.

While the sol-gel process offers control over size, shape, and composition, it can be difficult to achieve precise control. Additionally, changes in synthesis conditions, such as pH, temperature, and solvent choice, can have a substantial impact on the properties of the final product[55].

Furthermore, the nanoparticles tend to agglomerate due to high surface energy and Van der Waals forces, leading to poor dispersion in the liquid medium. This agglomeration can compromise reproducibility and effectiveness, potentially increasing toxicity. Recent studies have successfully reduced the lengthy processing times to a few hours, contingent on the materials utilized, pH level, and reaction temperature[58].

The chemicals required for the sol-gel process can be expensive. The coating or any produced material may shrink and crack, potentially compromising the integrity and performance of the final material. Also, some precursors used in the sol-gel process are toxic or hazardous, necessitating careful handling and disposal procedures[53]. Furthermore, the mechanical properties of materials produced via the sol-gel method may not be sufficient for all applications.

2.4. Methods of AR coatings deposition

2.4.1 Chemical Vapor Deposition

Chemical Vapor Deposition (CVD) is a common technique used for the deposition of thin films and nanoparticles onto various substrates through chemical reactions involving vapor-phase precursors[59]. In a typical CVD process, volatile precursor gases are introduced into a reaction chamber where they react or decompose upon contact with a heated substrate[60]. This results in the formation of a solid material that adheres to the substrate surface.

CVD encompasses thermal CVD, which utilises heat to decompose precursors; plasma-Enhanced CVD , which employs plasma to enhance chemical reactions at lower temperatures; metalorganic CVD, which involves metalorganic precursors for depositing thin films, particularly in semiconductor applications; and initiated CVD, which is a solvent-free technique that allows for the deposition of organic polymer films without the need for solvents.

The advantages of CVD are that the method allows high-purity deposits due to the controlled environment and removal of impurities. It can produce conformal coatings that uniformly cover complex geometries. The process can also be scalable for industrial applications, making it suitable for large-area substrates. The disadvantages of CVD are that the processes often generate toxic, corrosive, or explosive by-products, necessitating stringent health and environmental safeguards. This increases operational costs and complexity due to the need for specialized handling and disposal systems. Lastly, high temperature requirements, material stress, cost of precursors and the equipment complexity are some of the challenges experienced in CVD technique.

2.4.2 Electrochemical deposition

Electrochemical deposition is a powerful technique used to deposit nanoparticles onto conductive substrates, leveraging electrochemical cells to achieve precise control over the size, shape, and distribution of the nanoparticles[61]. This method has gained traction due to its ability to produce nanostructures with well-defined morphologies and minimal environmental impact. Electrochemical deposition involves the reduction of metal ions from a solution onto a conductive substrate, typically using a three-electrode setup. The substrate acts as the working electrode where nanoparticles are deposited, while the counter and reference electrodes complete the circuit.

Advantages of Electrochemical Deposition are its environmental friendliness, unlike chemical methods. The synthesis process can be completed quickly compared to traditional wet-chemical methods. Furthermore, with adjustments of parameters like current density and potential, it is possible to fine-tune the size and shape of nanoparticles.

Despite its advantages, electrochemical deposition faces several challenges such as reproducibility issues as the variations in experimental conditions can lead to inconsistent results, particularly in nanoparticle agglomeration and distribution. Lack of proper stability of nanoparticles and maintenance of uniform distribution on the substrate as uneven surfaces can lead to aggregation and reduced active surface area over time.

2.4.3 Physical Vapor Deposition

Physical Vapor Deposition (PVD) is a sophisticated technique used for depositing thin films and nanostructures onto various substrates[62], [63]. This method is pivotal in numerous industries, including electronics, optics, and aerospace, due to its ability to produce high-purity coatings with tailored properties.

PVD involves several key stages like evaporation, when the material to be deposited, typically in solid form, is heated above its melting point to generate vapour, which can be achieved through techniques such as thermal evaporation or sputtering[63]. It also involves transportation of the vaporized atoms through a vacuum environment towards the substrate. Moreover, condensation take place when the vapor reaches the substrates then forms a thin film that can range from a few nanometres to several micrometres in thickness. PVD also encompasses various methods, which includes sputtering, thermal

evaporation, and electron beam evaporation. PVD is widely used for coatings to create wear-resistant surfaces for tools and components, for producing anti-reflective coatings and mirrors and depositing materials for electronic devices and solar cells.

The advantages of PVD are that it produces a high-purity coating with uniform thickness and versatility. A wide range of materials, including metals, ceramics, and organic compounds, can be deposited using PVD techniques. Furthermore, compared to chemical deposition methods, PVD normally uses fewer hazardous chemicals, making it more environmentally friendly.

However, the disadvantages of PVD include the possibility of high costs, particularly for large surfaces and complex geometries. The PVD process can be expensive, particularly for large surfaces or complex geometry. PVD typically has limited thickness, often measuring less than a few microns. In addition, the PVD process necessitates complex and costly machinery, which requires trained personnel for operation and maintenance. This can be a barrier for smaller companies or those with limited budgets. Another challenge lies in the general restriction of the range of materials suitable for PVD to those capable of evaporating and depositing in a vacuum[62]. This limits the versatility of the coatings produced compared to other methods, such as chemical vapor deposition. Additionally, compared to some other coating techniques, the deposition rates in PVD are typically slower, potentially affecting efficiency in large-scale production environments.

In terms of environment, the high vacuum conditions required during the PVD process necessitate careful monitoring and control, adding complexity to the operation.

2.4.4 Spin coating

Spin coating is a widely used technique in materials science and engineering for creating thin, films on substrates[64]. During spin coating dispensing, a small amount of nanoparticle solution is placed onto the centre of a substrate. The solution typically contains nanoparticles suspended in a solvent.

The substrate is rapidly rotated around its axis and centrifugal force generated during spinning spreads the solution outward across the surface. As the substrate spins, the solvent evaporates, leaving behind a thin film of nanoparticles. The thickness of the film can be controlled by adjusting parameters such as spin speed, viscosity of the solution, amount of solution dispensed and spinning time[64]. After spinning, additional drying or curing processes may be employed.

The spin coating technique can produce uniform films with controlled thickness. It is **s**uitable for both small-scale laboratory experiments and large-scale industrial applications and can be used with a variety of materials, including polymers, metals, and oxides. In addition, the spin-coating method is known to have many advantages, such as being low-cost, simple, and requiring a low-temperature process[64].

The challenge is that spin coating typically handles one substrate at a time. This results in relatively low throughput compared to continuous methods like roll-to-roll coating, making it less suitable for large-scale production environments. Furthermore, a significant portion of the coating solution is ejected during the spinning process, leading to material wastage often exceeding 90% for some applications. This inefficiency can increase costs, particularly when using expensive materials.

Substrate size constraints and film thickness control are some of the challenges experienced during spin coating. In addition, in some cases, rapid drying induced by high spin speeds can hinder processes like self-assembly or crystallization that require more time to develop properly.

2.4.5 Dip Coating

Dip coating is a widely used technique for applying a uniform layer of material onto a substrate[65], [66]. This method is particularly effective for creating coatings with specific properties, such as enhanced durability, corrosion resistance, or functional characteristics[66].

The substrate, which can be made of various materials like metals, plastics, and ceramics, is first cleaned to remove any contaminants. This step is crucial for ensuring good adhesion of the coating. A suspension containing nanoparticles is prepared. These nanoparticles can be composed of metals, oxides, polymers, or other materials, depending on the desired properties of the final coating. The substrate is immersed in the nanoparticle suspension. The duration of immersion can vary based on the desired thickness and uniformity of the coating. After sufficient immersion, the substrate is withdrawn from the suspension at a controlled speed, with the faster withdrawal of the substrate, the thicker the film deposited[66]. This step is critical as it determines the thickness of the coating. Once withdrawn, the coated substrate is allowed to dry. Depending on the materials used, additional curing processes (such as heating) may be employed to enhance adhesion and finalize the coating properties.

With dip coating the controlled withdrawal allows for consistent thickness across complex geometries. Dip coating can be easily scaled for mass production.

Cost-Effective: Generally, requires less material compared to other coating techniques. The challenges experience with the process often requires a larger volume of coating solution than the substrate's volume, leading to significant wastage. This is particularly problematic in large-scale applications where cost efficiency is critical.

Contamination Risks -furthermore, the large reservoirs needed for dip coating can easily become contaminated, which may compromise the quality of the coating. This necessitates regular cleaning and maintenance, adding to operational costs.

Dip coating is limited to submersible parts as only components that can be fully submerged can be coated using this method. Inconsistent coating thickness, drying and curing challenges and batch processing limitations are also some of the disadvantages associated with dip coatings.

2.4.6 Spray coating with nanoparticle suspensions

Spray coating using nanoparticle suspensions is a versatile technique employed across various industries, including textiles, electronics, and biomedical applications. This method involves atomizing a suspension of nanoparticles and applying it to a substrate, resulting in a thin film or coating that can enhance the material properties of the surface.

The advantages of using nanoparticle suspension in spray coating are that spray coating using nanoparticle suspensions are designed to minimize material loss, resulting in reduced waste compared to traditional methods. This feature is essential for achieving desired functional properties, such as hydrophobicity or adhesion. Furthermore, nanoparticle suspensions can accommodate a broad spectrum of fluid viscosities, making them suitable for various substrates and applications.

Spray coating processes can be easily integrated into automated systems for large-scale production, making them suitable for high-volume manufacturing environments.

The disadvantages of using spray coatings are that the process can generate airborne nanoparticles, posing potential health risks to workers if proper safety measures are not implemented[67], [68]. Nanoparticles may agglomerate during suspension preparation or application, leading to inconsistent coating quality and performance. Ensuring uniform dispersion is critical but can be challenging. The effectiveness of spray coating with nanoparticle suspensions relies heavily on precise control of numerous parameters like nozzle pressure, distance from substrate.

Mesoporous silica coating which was fabricated by Manna S et al using spray coating techniques on a textured solar glass surface showed good hydrophobic, and abrasion resistance properties and achieved a transmittance of 86.83% [69].

2.5. Porous Silica

Silica particles are made up of silicon and oxygen, known as silicon dioxide (SiO_2), and commonly naturally acquired as quartz. Often referred to as silica, silicon dioxide is a crystalline or amorphous material consisting of a regular or irregular arrangement of repeating SiO_2 units. The sol-gel manufacturing method has been extensively utilised, wherein a precursor solution, solvent, and acid or basic catalyst are combined to yield the final material through a polycondensation reaction. Silicon alkoxides, specifically tetramethoxysilane (TMOS) and tetraethoxysilane (TEOS), are the main starting materials used to make sol-gel nanostructured silica materials.[70], [71], [72].

2.5.1 Composition and Structure

Elements: Silica is composed of silicon (Si) and oxygen (O) as shown in Figure 1.

Chemical Formula: The chemical formula for silica is SiO_2.

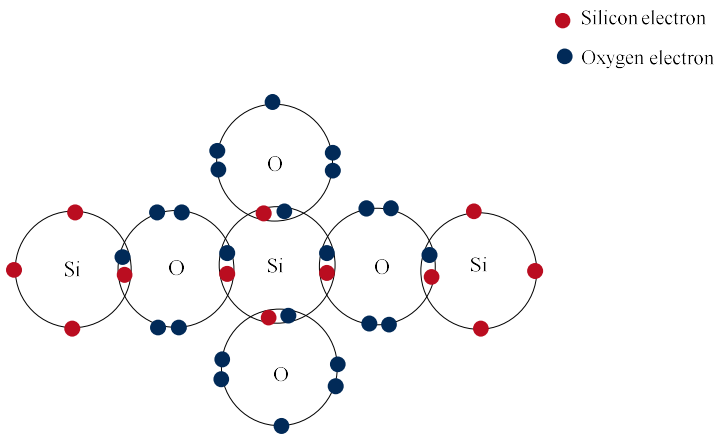

Figure 2 Atomic structure of silicon dioxide

Figure 3.1 Atomic structure of silicon dioxide

Silica is known to be stable under a wide range of temperatures and pressures, making it a common mineral in the Earth's crust[73]. Silica has various physical and chemical properties which make it suitable for nanotechnology and many other applications.

2.5.2 Physical properties of silicon dioxide

Silicon dioxide can be colourless to greyish and is found in crystalline or amorphous forms. It is typically odourless and tasteless. Furthermore, the density of silicon dioxide varies with its form, for example, α-quartz has a 2.648 g/cm³ density, while amorphous silica has a density of 2.196 g/cm[73]. The melting point of silicon dioxide is approximately 1,713°C, and its boiling point is around 2,950°C. The refractive index of silicon dioxide is about 1.46. Silicon dioxide has a low thermal expansion coefficient, which means it does not expand or contract significantly with temperature

changes. This property makes it useful in applications where thermal stability is crucial. It has a high dielectric strength, making it an excellent insulator in electronic applications. Silicon dioxide has low electrical conductivity, further supporting its use as an insulator in electronic devices. In its crystalline form, silicon dioxide forms a three-dimensional network of tetrahedra, where each silicon atom is covalently bonded to four oxygen atoms. The Si-O bond length is typically around 161 pm in α-quartz[74], [75].

2.5.3 Chemical properties of silicon dioxide

Silicon dioxide is generally unreactive due to its stable molecular structure. The molecule has a zero polarity because silicon forms two double bonds with oxygen, resulting in a stable configuration. It is highly stable under normal conditions and does not readily react with most acids or bases. However, it can react with hydrofluoric acid to form hexafluorosilicic acid. Silicon dioxide is practically insoluble in water and most acids, except for hydrofluoric acid. It can also dissolve in hot solutions of alkali hydroxides.

Silica has asymmetric stretching vibration modes, particularly in the Si-O-Si bonds, which correspond to mid-infrared wavelengths. The Si-O-Si bond angles of quartz (142°), cristobalite (150°), and fused quartz (143°) differ, according to diffraction data[76]. This stretching is due to a bridge of two silicon atoms connected by an oxygen atom, forming a Si-O-Si angle as shown in Figure 2.

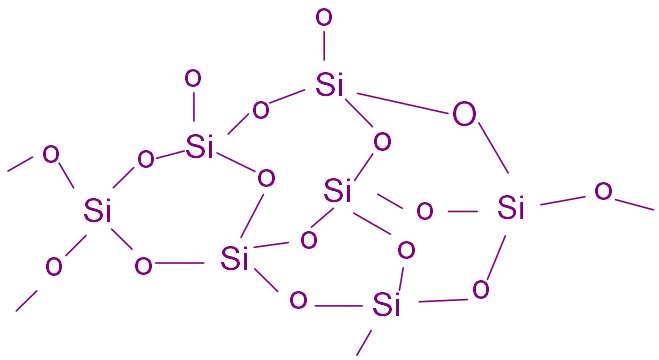

Figure 3 A microscopic structure of the silica with Si-O-Si bond

Silicon dioxide (silica) also plays a significant role in radiative cooling technologies due to its unique optical properties[77]. Radiative cooling is a passive technique that dissipates heat by emitting infrared radiation to the cold universe, particularly through the atmospheric transparency window (8–13 μm)[78]. Silica is widely used in radiative cooling because of its high emissivity in the mid-infrared region (8–13 μm), this emissivity depends on the thickness of the silica coatings applied[20], [79]. Silica is a passive radiative cooler as it does not require external energy input, and studies preferentially used it with Si_3N_4, and Al_2O_3 as multilayers to produce a substantial infrared emission[79]. However, bare silica films have a limitation due to an emissivity dip in the atmospheric transparent window. This can be improved by structuring the silica surface, such as using periodic deep gratings or cylinder arrays, to enhance emissivity and achieve better cooling performance

2.5.4 Amorphous silica

AR coatings for optical applications typically use amorphous silica rather than crystalline silica. This is because amorphous silica has a lower refractive index compared to crystalline forms, which is beneficial for AR coatings. The lower

refractive index allows for better matching between air and the substrate, reducing reflections. Furthermore, amorphous silica can form more uniform and smooth coatings compared to crystalline silica, making it easy to tune its structure to one's preference; this is important for optical applications where surface roughness can cause scattering.

The porous nature of amorphous silica coatings can also be controlled to fine-tune the refractive index. This allows for the optimization of the AR properties. Amorphous silica can be easily deposited using various methods like sol-gel processes, which are commonly used for AR coatings. The structure of amorphous silica allows for easier incorporation of other materials or modifications to enhance properties like durability or self-cleaning capabilities. Its nanoparticles can be used to create nanostructured AR coatings with enhanced performance.

2.6. Combination for AR coatings and radiative cooling coatings for solar photovoltaics

Recently, there has been an emerging trend of AR coatings being designed to simultaneously increase reflectance of sunlight and radiating heat through mid-infrared wavelengths, which is known a passive daytime radiative cooling (PDRC). These studies have been done for various purposes, like for indoor cooling or light management. For example, a study demonstrated that a metamaterial could achieve a temperature reduction of 6°C below ambient levels, showcasing its potential for energy-efficient cooling solutions[80]. This thermal cooling is according to thermodynamic principles where two object with different temperature exchange heat through thermal radiation until they reach temperature equilibrium. The heat is transferred from a warmer object to a cooler object, this is as stated by Stefan-

Boltzmann law of radiation in equation 4, where E is the radiant heat energy emitted per unit area, σ is the is the Stefan-Boltzmann constant $5.670374419 \times 10^{-8} W/m^2K^4$ and T is the absolute temperature in kelvins.

$$E = \sigma T^4 \qquad (4)$$

In solar photovoltaics, the aim is to increase the transmittance of light in the spectrum range (300 nm- 1100 nm) and increase the radiation of heat to the cold outer space through the atmospheric transparency window (8 -13 μm). Even though various thermal cooling methods have been developed, like active cooling, they mostly require energy some energy input, which makes it even less efficient, as some of the generated energy is used to cool the solar PV modules[4], [31], [81].

Some studies focused on the fabrication of porous coatings, although the challenge in porous coatings is that they do not function well when exposed to dust accumulation and water wetting. To solve the wetting and dust problem, some researchers solve this by making the coatings hydrophobic[82].

In a study, related to passive radiative cooling of solar PV module, a hexagonal silica array of cylinders was etched into the surface of silica solar module glass[83]. In the study emissivity was increased to 97.7% from 84.3% in the mid-infrared range (7.5 - 16 μm), without hindering light transmission[83]. The cooling potential of 21 K was observed in the study compared to the bare silicon reference.

It is known that the emissivity of thermal radiation increases with the increase in the size of the particles. Although as the pore sizes and porosity increase, transmittance of the coating also increases. Thermal cooling of the particle size and the anti-reflection

of light seems to be inversely proportional. Since the thermal cooling decreases with the decrease in particle size, the particles' anti-reflecting property increases with the decrease in particle size.

However, as the particle size decreases to less than 2 nm, it gives rise to an increase in the refraction index, which hinders the anti-reflective properties of the materials as more light gets scattered within the bulk particles of the material instead of being transmitted.

Current studies remain limited regarding how porosity variations in silica coatings influence mid-infrared radiative properties. While existing hypotheses suggest that emissivity correlates with coating thickness, thicker layers potentially enhancing infrared radiation, parallel observations indicate that thinner coatings may improve transmittance. These interdependent thickness effects create critical uncertainties in optimising silica-based thermal management systems. This investigation aims to resolve these ambiguities by systematically analysing how porosity gradients and layer thickness interact to govern mid-infrared emissivity and transmittance, thereby advancing functional design principles for silica coatings in enhancing solar photovoltaic efficiency.

Chapter 3

Research Methods

The study fabricated and characterised the porous silica coatings

3.1 Experimental procedures in the fabrication of silica sol for porous silica coatings

This study synthesised three silica sols using a base/acid double catalysis process. This base/acid double catalysis involves preparing two separate sols: one with hydrochloric acid as a catalyst and another with ammonium hydroxide[72], [84]. The two sols were combined and aged for 24 hours before spin coating. The chemicals waste and all waste generated in this study were disposed according to the KIT-Campus North waste disposal regulations.

The synthesised silica sol conforms to the chemical equation 5, which encompasses two primary steps: hydrolysis and condensation involving TEOS, distilled water, ethanol, Pluronic F127, ammonium hydroxide and Hexamethyldisilane (HMDS).

$$Si\,(OC_2H_5)_4 + 4\,H_2O \rightarrow SiO_2 + 4\,C_2H_5OH \qquad (5)$$

3.1.1 Apparatus used in the fabrication of porous silica coatings

The chemical process was conducted in a closed system for better control over the reaction conditions. The study used chemicals listed in Table 1 and materials given in Table 2

Table 1 Shows the list of chemicals used in fabricating the porous silica coating

Chemical list	**Quantity**
TEOS 99.9%	200 ml
Ethanol 99.9%	1 l
Distilled water (H_2O)	200 ml
Pluronic F127	8g
Diluted Hydrochloric Acid (0.1M)	100 ml
Ammonium hydroxide	100 ml
HMDS 99.9%	30 ml

Table 2 Shows materials and apparatus used in the sol-gel process of fabricating nanoparticles for AR coatings

Materials	**Quantity**	**Volume (ml)**
Three round-bottom flasks	1	250
Magnetic Stirrer	2	-
Beaker	1	250
PH paper	>20	-
Pipette	>10	5
Balance scale	1	-
Thermometer	1	-
Glass bottle	2	250
Glass bottle	1	500
Elastomer septum	3	-
Glass rod	2	-

3.1.2 Step-by-step procedures used in the fabrication of porous silica

The chemical process was conducted as seen in the schematic figure 4 below, where part 1 is base catalysed sol and part 2 is acid catalysed sol which later were combined as seen in this schematic.

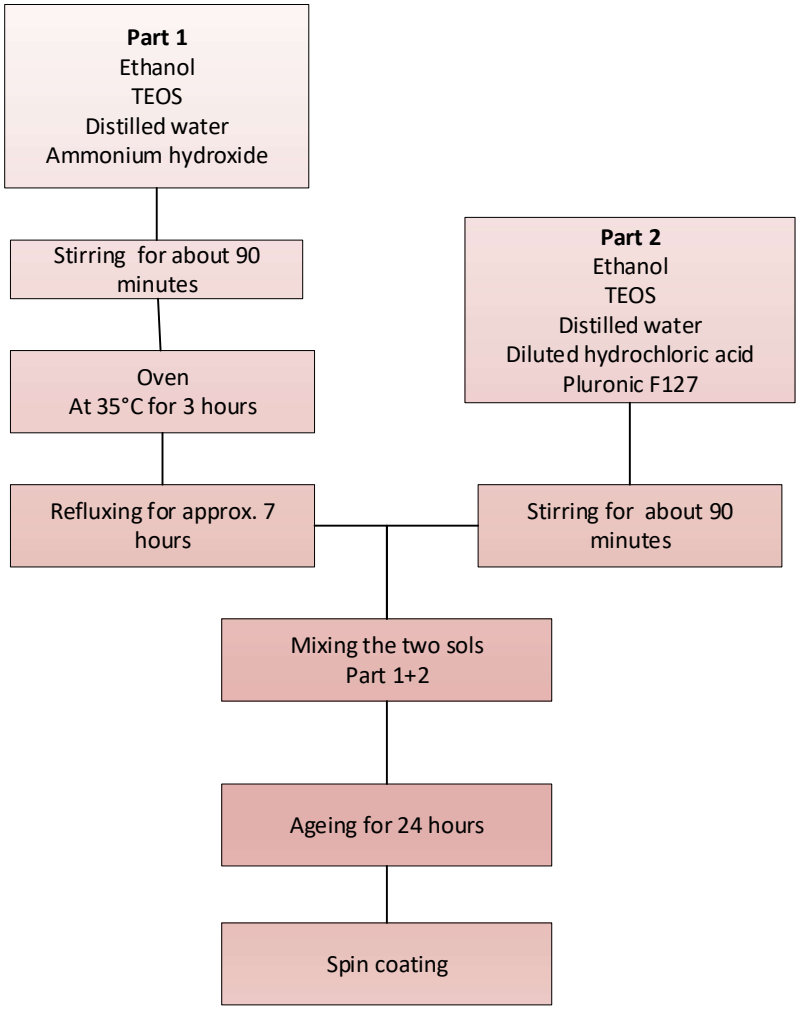

Figure 4 A schematic diagram showing the two sol when synthesised and combine before spin coating

Part 1 Preparation of the base catalysed sol

The base-catalysed sol was prepared with an approximate total volume of 150 ml of TEOS, ethanol, and water (20, 115, 8 ml, respectively), excluding the Pluronic F127

mass and the volume of ammonium hydroxide. This sol was prepared using the chemicals in Table 1 and the apparatus in Table 2 and the set up as shown in Figure 4. Since the volume of ammonium hydroxide was not known earlier on, the sol's pH was known to be 10, so the ammonium hydroxide was added while testing until the sol reached pH 10.

The instruments were cleaned with water and ethanol and subsequently dried before use to minimise contamination. Initially, 20 ml of TEOS was added into a 250 ml three-neck round-bottom flask. After adding TEOS, 115 ml of ethanol was incorporated into the same bottom flask and stirred well using a magnetic stirrer for 5 minutes at room temperature.

Following the addition of TEOS and ethanol, the solution was heated to 60 degrees before 8 millilitres of water was added. Even while heating, the sol was stirred. Five millilitres of ammonium hydroxide were added dropwise until the pH of the sol reached ten. As illustrated in Figure 4, the chemical reaction was carried out in a closed system with a bottom flask connected to a vertical condenser because heating was required, to retain the same volume of chemical input and to prevent the influence of external surroundings on the chemical reaction. To prevent chemical evaporation during the chemical process, a condenser was attached vertically with cold water flowing to cool the vapour. A thermometer was placed in the flask on the left to measure the temperature. The system which was closed with a septum was only opened when distilled water and ammonium hydroxide were added, and when testing the pH.

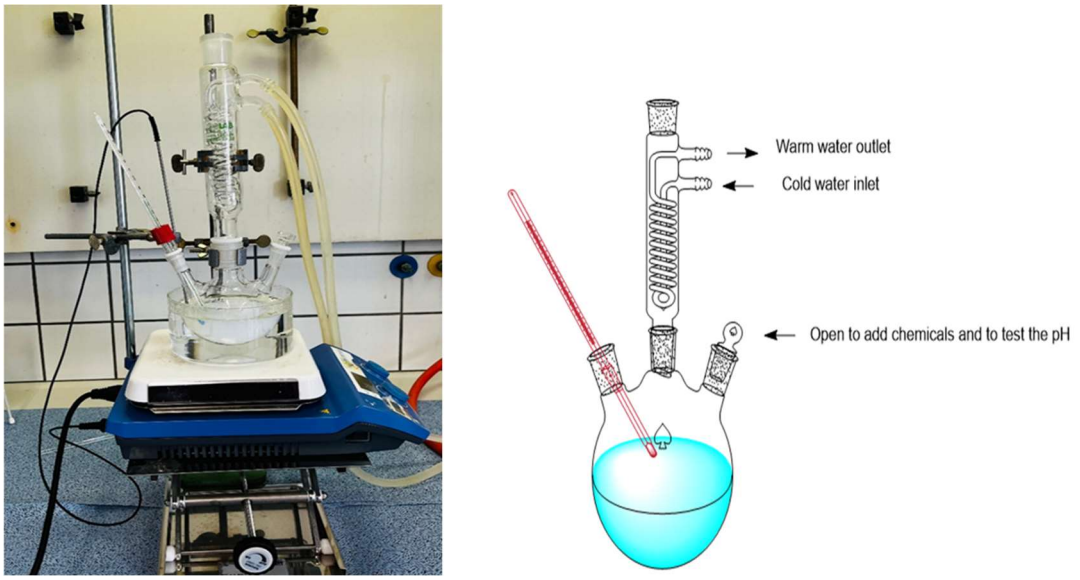

Figure 5 Base catalysis actual setup (left) and a schematic view of the chemical reaction setup(right)

The final pH for the sol set to around pH 11, the pH level plays a significant role in determining the kinetics of the sol-gel process. The pH number was determined by using the pH paper to test the pH as shown in Figure 6. Various pH papers of three types were used to obtain accurate results as seen in Figure 6 (right).

Figure 6 Three types of pH paper used in this study(left) and measuring the pH of a sol using a pH paper (right)

Later the sol was removed from the bottom flask and transferred to a 250 ml glass bottle, the bottle was then transferred to an oven and kept at a temperature of 35 ℃ for

three hours. The sol was put in the oven to speed up the ageing of the base catalysed sol.

After removing the sol from the oven, it was transferred back to the three-neck rounded bottom flask. The set-up was reconnected, and the temperature was adjusted to 86℃ on a hot plate for the reflux process to take place. The steady reflux temperature in the sol was recorded at 76℃.

The purpose of the reflux was to remove ammonium from the sol because it can have a detrimental effect on the AR coating. Furthermore, it took nearly six hours for the reflux process to completely remove ammonium; this was monitored using a pH paper continuously until the pH reached 7, which denotes a neutral solution.

Part 2 Preparation of the acid-catalysed sol

Part 2's total volume was roughly 100 ml, with the volume ratio in millilitres for TEOS, ethanol, and water being 5:80:3. This sol was prepared using the chemicals in Table 1 and the apparatus in Table 2. Hydrochloric acid was used as a catalyst in the acid-catalysed solution. The 250 ml beaker was first cleaned with ethanol and allowed to dry before adding 77 ml of ethanol and 3 ml of distilled water with a pipette. The mixture was stirred with a magnetic stirrer. On the other hand, 0.25 grams of Pluronic F-127 were weighed and placed in a separate 50 ml beaker, followed by 3 ml of ethanol in the same beaker, and the mixture was stirred for 20 minutes. The sol was then mixed with ethanol and water in a 250 ml beaker using a magnetic stirrer. While stirring, 5 mL of TEOS was added to the mixture with a pipette, followed by more than 5 mL of hydrochloric acid to function as a catalyst.

A pH paper was used to measure the pH of the sol; by immersing a glass rod tip in the sol and then rubbing it on a pH paper, the pH was obtained instantaneously, and multiple pH papers were used for reliable pH readings. The acid was added until pH 2, following which it was left to stir as shown in Figure 6, it was left to stir for around 60 minutes.

Figure 7 Acid-catalysed sol setup

After parts 1 and 2 were completed, as shown in Figure 7, the two sols were blended in a 500 ml bottle as shown in figure 8, stirred at room temperature for at least 2 hours, and left to age for one day at room temperature.

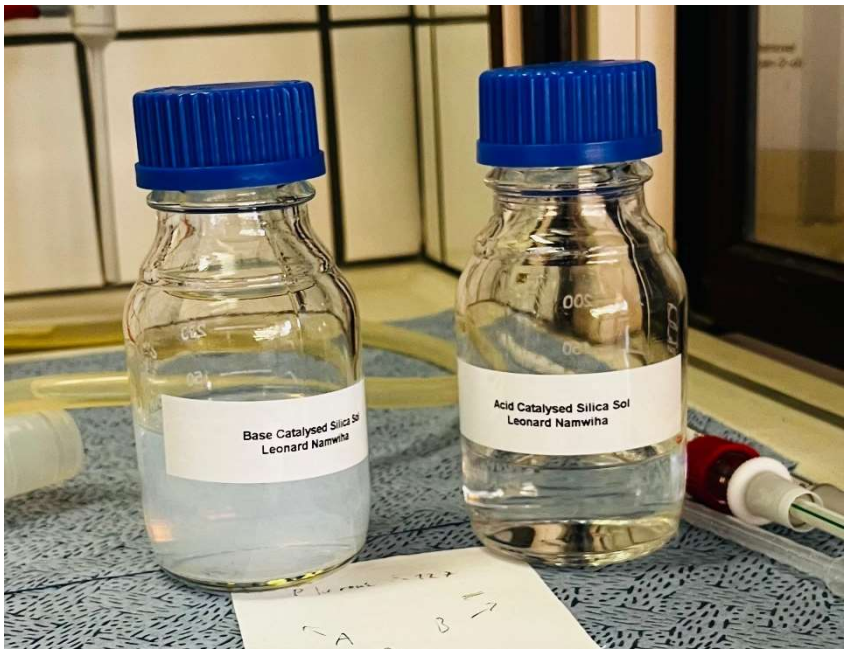

Figure 8 Base-catalysed sol and Acid-catalysed sol

After ageing for 1 day, the sol was then taken for the spin-coating process. The trial was repeated twice with only changes made to the amount of Pluronic F127 used: 0.40 g and 0.60 g. The aim of repeating the chemical process with different amounts of Pluronic F127 was to obtain porous silica coatings with different porosities.

Pluronic F-127 is a triblock copolymer consisting of a central hydrophobic block of polypropylene glycol flanked by two hydrophilic blocks of polyethylene glycol (PEG)[85], [86], [87]. It is a non-ionic surfactant with both hydrophilic and hydrophobic properties. Pluronic F-127 is commonly used in silica sol-gel as a templating agent, increasing silica particles' pore sizes by even 8nm[87].

The total volume for both steps part 1 and part 2 was estimated to be 250 ml with the total final volume ratio for TEOS, ethanol, and water to be 25:198 and 15 (ml) respectively.

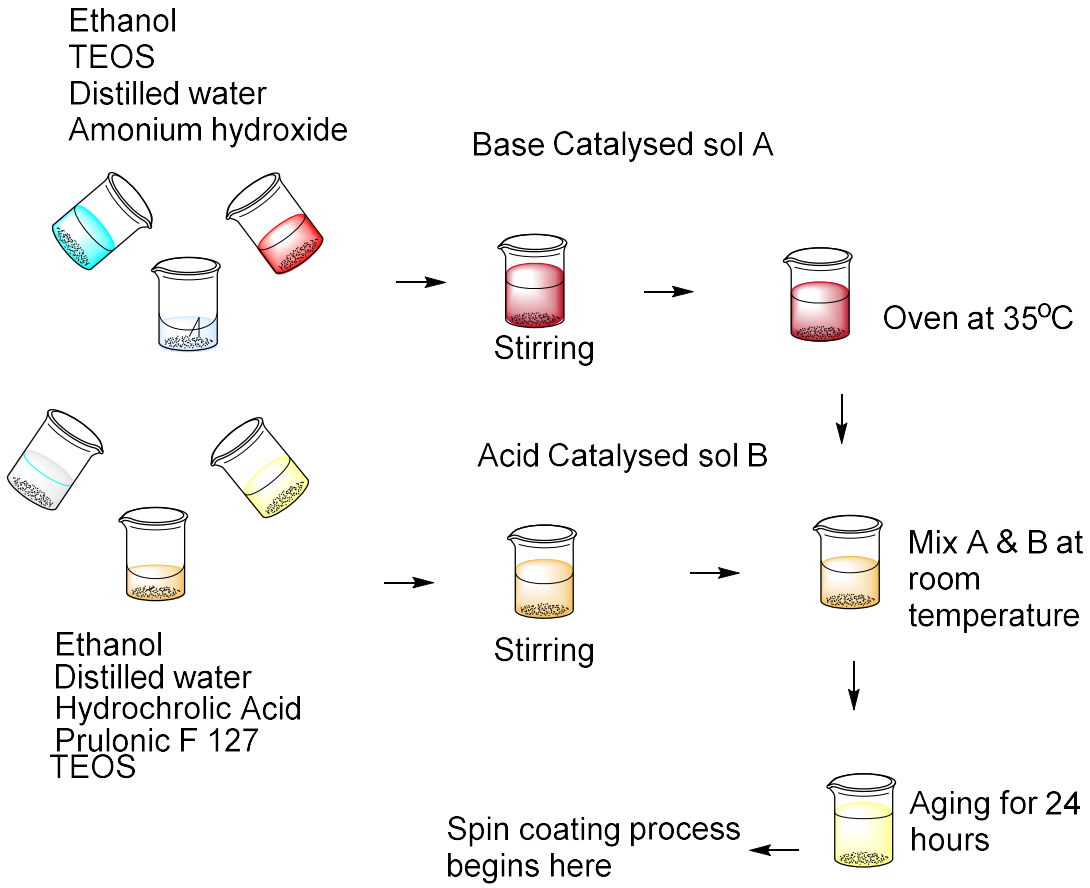

Figure 9 The chemical process schematic view in full detail including both steps

In figure 9, the schematic view show how the process was conducted; it does not show the actual apparatus used but instead just uses beakers and different colours to represent the idea behind of different chemicals used.

The setup was completely the same for all three trials with only a few adjustments in the amount of PF127. The time duration for each trial took three days, the first day was

a day of the chemical process which starts early in the morning at 08:30 am, with the first phases taking about 2h30 minutes and then followed by the ageing of Part A sol in the oven for 3 hours. The reflux stages took different times due to the amount of ammonium hydroxide added to the solution, with the first trial taking about 11 hours to remove ammonia, the second phase taking approximately 8 hours and the third phase taking about 7 hours 30 minutes.

The removal of ammonia through refluxing reduces the pH of the solution from around 11 to neutral (pH 7). This pH adjustment is crucial for preparing a stable sol-gel coating solution that can be effectively applied onto glass optics through spin-coating or dip-coating techniques[88]. Figure 10 below shows all the silica sols prepared in this study.

Figure 10 All the silica sols prepared in this study

To minimise contamination during this whole process, hand gloves where utilized and material used where all kept free from being contaminated, during handling and storage.

3.1.3 Spin coating and sintering of porous silica coatings

The spin-coating process involves four stages of deposition: spin-up, spin-off and evaporation, with the main stages as shown in figure 11 below.

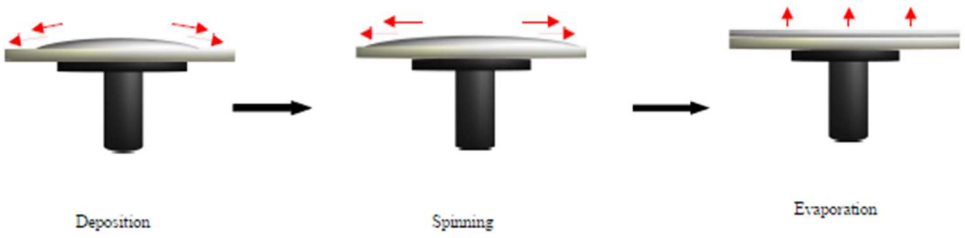

Figure 11 The schematic view of the spin coating steps

The sols prepared in this study were then spin-coated on soda-lime glass substrates with 1 mm thick and 3 mm in diameter[27]. To minimise contamination during this coating and sintering step, hand gloves where utilized, the material used where all kept clean and free from contamination.

During spin coating about 0.5 ml of the sol was taken using a pipette and dispensed on a glass substrate low iron glass. Before spin coating the spin, coater was set to 500 rpm speed for 30 seconds and the sol was deposited during this stage call known as dynamic dispersion it was then increased to the s speed of 1500 rpm for 20 seconds, as the program used is seen in a Figure 12.

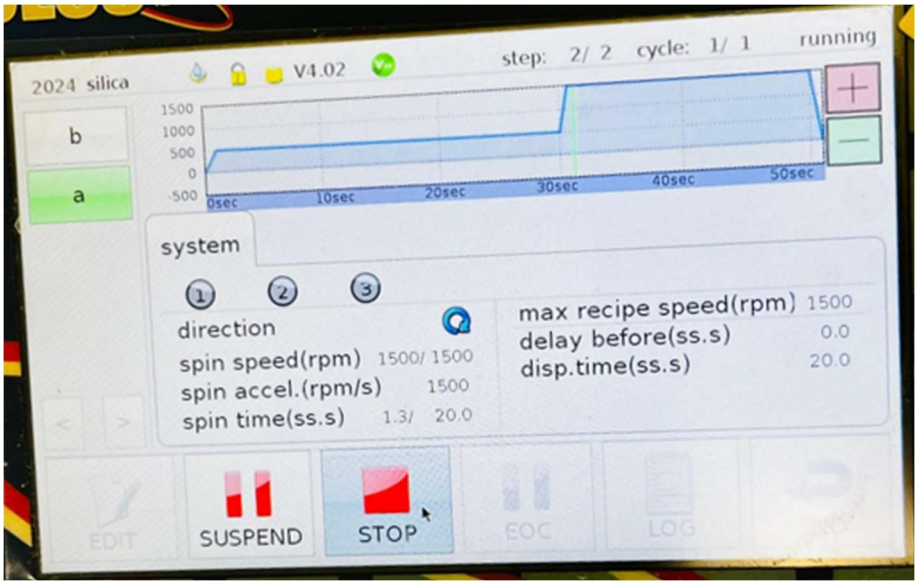

Figure 12 This diagram indicates a program that was set for the spin coating of all samples

During spin coating, 1 layer, 2 layers and 3 layers of porous silica coatings for each layer were applied there was a five-minute period for the layer to dry at room temperature before applying another layer. After spin coating, the samples were then taken for sintering in the oven microwave oven (shown in Figure 12) up to the temperature of 450 for 1 hour at a ramping rate of 5 ℃/minutes.

Figure 13 Sintering oven used in this study

After sintering the fabricated coatings as shown in Figure 13, the coatings were taken for the characterisation step and testing. Images of the nine fabricated silica coatings are shown in Figure 14 below.

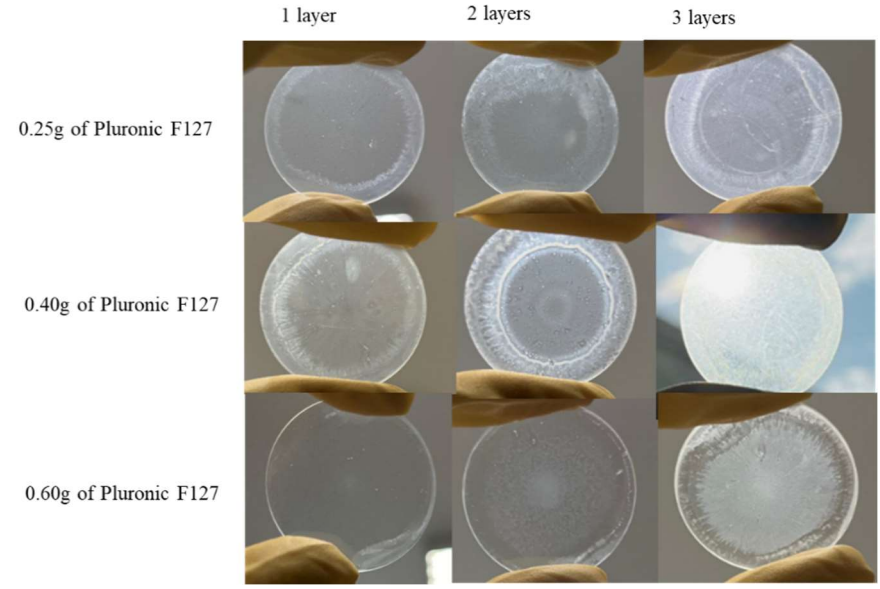

Figure 14 Actual pictures of the porous silica coatings fabricated in this study

3.2. Characterisation of the porous silica coatings fabricated in this study

The sizes and thickness of the porous silica coating particles were measured with a scanning electron microscope (SEM). The transmissivity and emissivity properties of the porous silica coatings fabricated in this study were tested using Fourier transform infrared (FTIR) and ultraviolet-visible-near infrared spectroscopy (UV-Vis-NIR).

3.2.1. Scanning Electron Microscopy (SEM)

SEM is an advanced imaging technique that employs a focused beam of high-energy electrons to examine the surface of a specimen. This method offers detailed information about materials' morphology, composition, and crystalline structure, achieving high resolution in the imaging process. The working principle of SEM is based on the interaction between the electron beam and the atoms in the sample[89].

When the electron beam impinges on the specimen, several types of signals are generated due to electron-specimen interactions. In the electron gun of the SEM above the column, electrons are produced and accelerated to 0.1-30 keV[90]. The electron beam from the hairpin tungsten gun has a large diameter, making it unable to create a high-resolution image. Apertures and electromagnetic lenses are used to concentrate and define the electron beam and produce a tiny electron spot on the specimen. For tungsten filaments, the electron source is about 50 μm. It is demagnified to provide the required spot size (1-100 nm). For electrons to be transferred without air scattering, a high vacuum is required[91]. Photographing and observing the specimen surface in real-time is made possible by the processing system, electron beam scanning coils, signal detection, and specimen stage[89].

3.2.2. UV-Vis-NIR Spectroscopy

UV-Vis-NIR spectroscopy is a powerful analytical technique used to measure the absorbance, transmittance, and reflectance of materials across the ultraviolet, visible, and near-infrared regions of the electromagnetic spectrum[92]. The operation of UV-Vis-NIR spectrophotometers is primarily based on the Beer-Lambert Law, which states that the absorbance (A) of light by a sample is directly proportional to both the

concentration (c) of the absorbing species and the path length (l) through which the light travels as shown in equation 5:

$$A=\varepsilon \cdot c \cdot l \qquad (5)$$

Where A = Absorbance, ε= Molar absorptivity coefficient c = Concentration of the absorbing species and l = Path length of the sample

UV-Vis-NIR Spectrophotometer consists of a light source that emits light across the desired wavelengths. Common sources include Deuterium lamps for ultraviolet light, Tungsten lamps for visible light, and Halogen lamps for near-infrared light.

Additionally, it has a monochromator, which chooses which light wavelengths to let through the sample. It uses diffraction gratings or prisms to break up incoming light into its individual wavelengths. a sample cell that contains the sample that light travels through. For measurement consistency, the path length is usually set at 1 cm. A detector that produces an electrical signal from transmitted light. For low-light detection, photomultiplier tubes (PMTs) are a common detector; for wider applications, photodiodes and charge-coupled devices (CCDs) are used. Absorbance data is shown by a readout device, frequently using computer software that enables additional analysis and comparison with established standards. The light source creates a beam that travels through the monochromator, which separates wavelengths, as part of an operational workflow for light emission.
Depending on the characteristics of the sample, some light is absorbed when the chosen wavelength interacts with the sample in the sample cell. The detector receives the remaining light and converts it into an electrical signal. After processing this

signal, the readout device generates a spectrum or absorbance values that may be examined to determine both the sample's qualitative and quantitative characteristics.

3.2.3. Fourier Transform Infrared Spectroscopy

FTIR is a powerful analytical technique for identifying and characterizing materials based on their molecular vibrations. The technique relies on the interaction of infrared (IR) light with matter, providing insights into molecular structure and functional groups[93]. The core principle of FTIR spectroscopy is based on the absorption of infrared radiation by molecular bonds, which causes them to vibrate at specific frequencies. Each type of bond absorbs IR radiation at characteristic wavelengths, allowing for the identification of functional groups within a molecule.

3.3. Characterisation of the hydrophobicity and hardness of the fabricated coatings

The hydrophobicity initially involves measuring the contact angle of the fabricated thin film with a higher contact angle > 90°, indicating that the thin film is hydrophobic (low wettability) and a lower contact angle < 90°, indicating that the thin film is hydrophilic (high wettability)[94]. After immersing the fabricated coatings in the HMDS solution for 5 minutes, they were heated on a hot plate. Subsequently, less than 0.5 ml of water was dropped onto a thin film using a pipette to observe the hydrophobicity properties.

A pencil test allows the study to determine the mechanical strength of the fabricated coating. However, even without conducting a pencil test, it is observed that the

coatings exhibit good mechanical properties. The mechanical assessments address the coating strength and adhesion of the deposited films to the substrate. To achieve coatings with strong mechanical properties, an acid-catalysed sol is used, which is believed to enhance the adhesion of the coatings to the substrate (glass)[95].

Furthermore, to assess the hardness of the thin films using a pencil test technique, various pencils are used in this process. Pencils named 9H, 8H, 7H and 6H can be used to test for the mechanical strength of the thin film as follows[96]: The pencil is held at a 45° to the film surface. By applying a consistent force and drawing a line approximately 1 cm in length on the thin film surface with different pencils until the pencil that scratches the surface is observed, a record of the pencil is then noted. It is noted that the tests begin with the softer pencil with the hardest pencil known to be 9H.

This study uses base/acid catalysis which are known to result in coatings with high hardness and good mechanical strength[19], [74]. The mechanical test was not conducted (severe time limitations on fabrication of all specimen and assessment of all their other properties made it virtually impossible to finalise this test because the specimen had to be left at KIT (Germany) before I returned to Namibia). The assertion of high mechanical strength and abrasion resistance of the coatings fabricated in this study is based on the method of their fabrication and is strongly supported by theory and literature[17], [19], [74], [95], [97]. Further justification for the mechanical strength and abrasion resistance of the coatings is provided by the fabrication method employed in this study. Acid catalysis promotes the formation of branched, cross-linked Si–O–Si networks through protonation of alkoxy groups, which accelerates hydrolysis and condensation. This process generates abundant

silanol (Si–OH) groups that react with hydroxyl groups on the glass substrate surface, resulting in the formation of high-density Si–O–Si bridging bonds at the film–substrate interface. Hence this leads to a highly adhesive and mechanically robust silica coating. The study would also not carry out the pencil test due to the short time limit that was set to conduct, and research was left with the institution of host. However, the mechanical robustness may only be affected or compromised with the increase in porosities or further increase in pores that lower the refractive index and increase the transmittance. In this study it was not possible to measure the refractive index of the coating due to unavailability of measuring equipment.

Chapter 4

Results and Discussions

This chapter presents a detailed analysis of the characterisation results of the coatings fabricated in this study, as well as a discussion of the results.

4.1 Assessment of the thickness, shape and sizes of the porous silica coatings

4.1.1. Presentation of results:

Six out of the nine coatings fabricated in this study were examined using SEM to evaluate their morphology, particle sizes, and thicknesses. The findings and discussions regarding the SEM images of the porous silica coatings fabricated in this research are presented below. This includes an analysis of surface uniformity at various viewing distances, a review of particle sizes, and an assessment of the thickness of the fabricated coatings. As observed in Figure 15, the spin-coating technique successfully

produces thin films with a uniform structure.

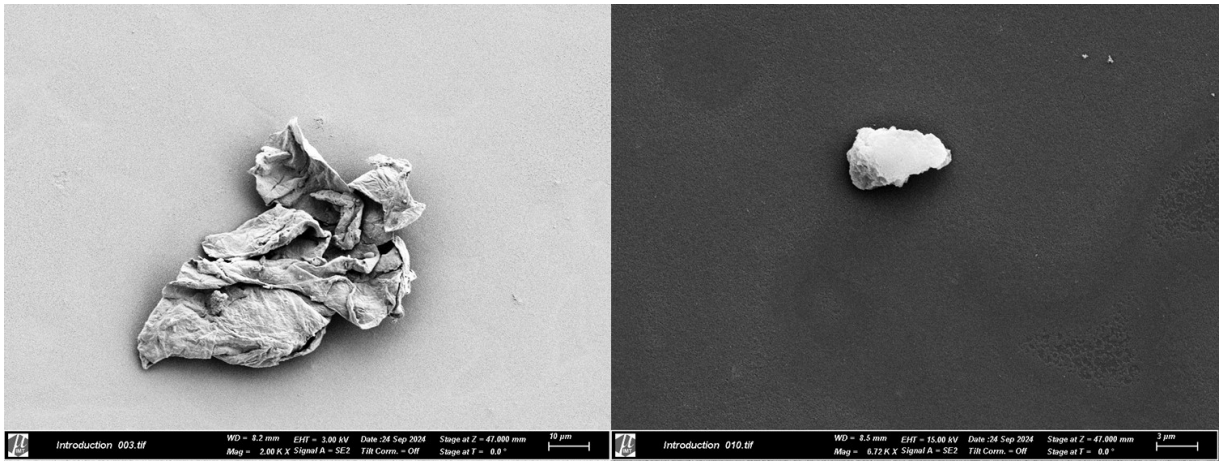

Figure 15 SEM image showing surface uniformity of the 1-layer porous silica (0.40 g Pluronic F127) coatings at 10µm and 3µm viewing distance, respectively

The images in Figure 15 start with a view of a porous silica surface at 10µm. On the left, the uniform surface morphology of the fabricated coatings is indicated. Additional SEM images of the same coatings are presented in Figures 15, which display the sizes of the fabricated nanoparticles.

The SEM results in Figure 15 illustrate the diameters of the fabricated silica particles. The observations indicate that the particles have thicknesses of 52.74 nm, 79.12 nm, and 55.67 nm, resulting in an average thickness of approximately 62.51 nm for the fabricated particles. These particles fall within the suitable range for anti-reflective coatings. However, some studies suggest that smaller particles, typically ranging from

10 nm to 30 nm, are more effective due to the way larger particles scatter light[30], [98].

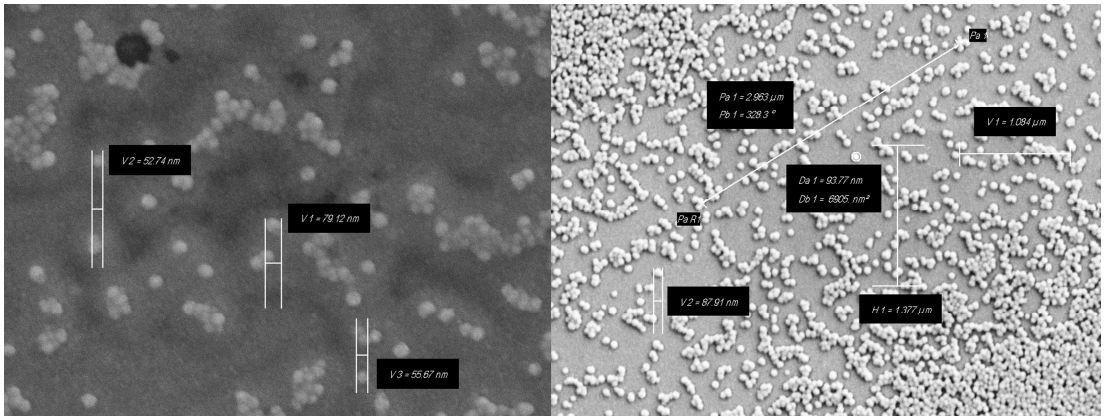

Figure 16 SEM image showing the diameter of the nanoparticles in the fabricated porous silica coatings

By examining the particle sizes in Figures 16, the study successfully produced spherical particles using base catalysis with ammonium hydroxide. In contrast, acid catalysis does not yield spherical nanoparticles within a short aging period; instead, it tends to result in a polymeric structure[99].

The study primarily utilizes acid catalysis (specifically, a combination of base and acid catalysis) to create a coating that forms a strong bond with the substrate (glass). This is because acid demonstrates superior adhesive properties compared to base catalysis, making the coating less likely to be scratched off the substrate[74]. The thickness of the porous silica coatings fabricated in this study was assessed using an SEM. The results obtained in the study only focused on six coatings, mainly for 1-layers and 3-layers, leaving out 2 layers since 1 and 3-layers are seen to be more interesting to measure, making a 2-layer thickness easily predictable.

The thin film, thickness was measured using a SEM as it can be observed in Figure 17. The thickness of one layer for 0.25 was observed to be 754.5 nm and the thickness of

the three layers of porous silica coatings, made with the silica sol containing 0.25 g of Pluronic, was measured to be approximately 1.135 μm.

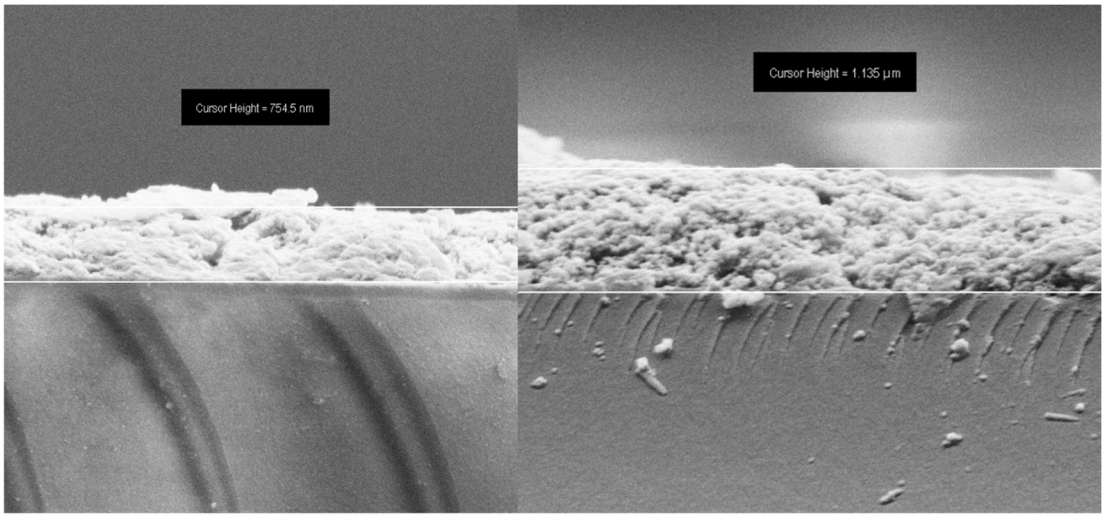

Figure 17 The thickness of the 1-layer (a) and 3-layer (b) of porous silica coatings fabricated from silica sol containing 0.25 g of Pluronic F127

The thickness of a one-layer thin film fabricated using a sol containing 0.25 grams of pluronic F127 is illustrated in Figure 17. This coating was applied to a glass substrate at a spin speed of 1500 rpm, which is known to be suitable for depositing thin films that are thicker than the measured thickness of 754.5 nm. The achieved thickness may be attributed to the lower viscosity of the silica sol used in this coating, which may be caused by more silica content and less porosity due to less Pluronic F127 content. This because high viscous silica sol can produce thicker coating because they resist flow more during the spinning process, leading to less material being flung off the substrate, and lower viscous silica sol can produce silica sol with thinner thickness after spin coating as they flow more easily[100].

When comparing the thicknesses of the single layer depicted in Figure 17 to the thickness of the three layers, it is evident that the thickness of the three layers is not even double that of the single layer. One possible reason for this inconsistency may be the viscosity of the sol; using less pluronic F127 could result in a sol with lower viscosity, which would lead to thicker coatings that are uneven in thickness.

The thickness of the porous silica coatings fabricated with silica sol containing 0.40 g of pluronic F127 was measured using SEM, as shown in Figures 18.

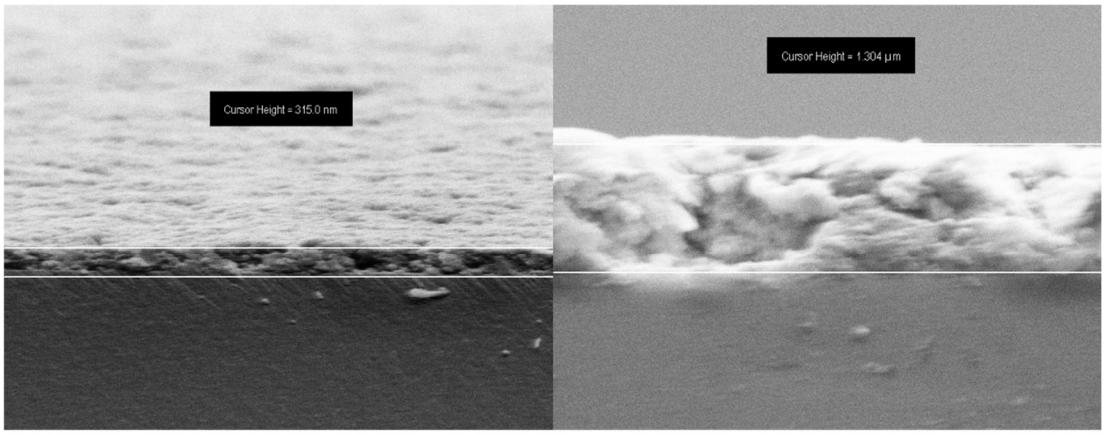

Figure 18 The thickness of the 1-layer (a) and 3-layer (b) of porous silica coatings fabricated from silica sol containing 0.40 g of Pluronic F127

The one-layer coatings shown in Figure 18 have a thickness of 315 nm, while the three-layer coatings have a thickness of 1.304 µm.

The results indicate a significant difference in thickness, with the three-layer coating being over 900 nm thicker than the one-layer coating. Specifically, the thickness of the three-layer coating is approximately four times that of the one-layer coating. This variation can be attributed to the viscosity of the sol and the spin coating technique,

which may be influenced by factors such as spinning speed and drying time between the application of layers.

In the experiment involving porous silica coating layers fabricated with a silica sol containing 0.60g of Pluronic F127, the single-layer porous silica coating achieved a thickness of 199.9 nm, as illustrated in Figure 19. In contrast, the thickness of the three-layer porous silica coatings Figure 19 measured 959.7 nm. Upon examining the thicknesses obtained in this trial, it is evident that the thickness of the single layer is approximately one-fourth that of the three-layer coating. Although one might expect the thickness of the three layers to be roughly three times the thickness of the single layer, the actual measurement deviates from this expectation, indicating that the relationship is not strictly linear.

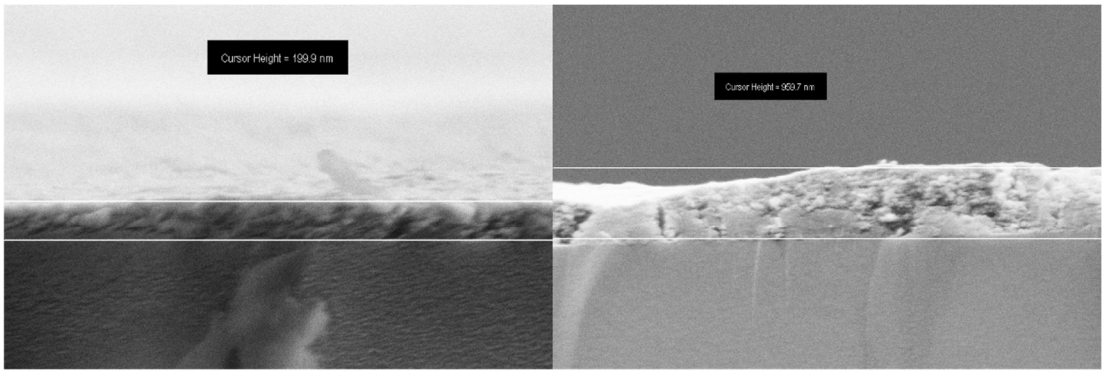

Figure 19 The thickness of the 1-layer(a) and 3-layer (b) of porous silica coatings fabricated from silica sol containing 0.60 g of Pluronic F127

In summary, the thickness of the porous silica coatings fabricated with 0.25 g of pluronic is 754.5 nm for a single layer and 1.305 μm for three layers. For the coatings made with a silica sol containing 0.40 g of Pluronic, the thicknesses observed were 315.0 nm for one layer and 1.304 μm for three layers. Additionally,

the coatings fabricated with a silica sol containing 0.60 g of Pluronic exhibited thicknesses of 199.9 nm for a single layer and 959.7 nm for three layers. The thickness results show a decrease in the thickness as the pluronic F127 amount increases, this can be seen when the single layer thickness moved from 754.5 nm for an amount of 0.25 g to 199.9 nm for and amount of 0.60 g.

These measurements support previous literature suggesting that with a spin speed of 1500 rpm, it is possible to achieve a thickness of around 200 nm. However, it is essential to consider factors such as the viscosity and chemical composition of the silica sol, which can affect the final thickness[100].

4.1.2. Discussions

The preparation of the coatings in this study yields a porous silica coatings as it can be observed by the SEM images figures 15-19. The study utilised the chemicals TEOS, Ethanol and Ammonium hydroxide for the following reasons:

TEOS, a silicon alkoxide, undergoes hydrolysis and condensation reactions to form SiO_2[101]. It serves as the primary source of silicon in the sol-gel process, enabling the formation of a silica network essential for AR coatings. The concentration of TEOS affects the viscosity of the sol and the time required for gelation. Higher concentrations of TEOS can lead to increased viscosity and faster gelation times, which are critical for controlling the thickness and uniformity of the AR coatings. It can affect the hardness and density of the gel, as the presence of terminal Si-OH bonds increases both properties. This is important for the durability and effectiveness of AR coatings. Excessive addition of TEOS can lead to phase separation, which impacts the microstructure of the gel. This phase separation can be attributed to the

self-condensation of TEOS, affecting the uniformity and optical properties of the AR coatings.

Ethanol was used as a solvent in the silica sol-gel process. It helps to dissolve the silicon alkoxide precursors and facilitates the hydrolysis and condensation reactions that form the silica network. The presence of ethanol can influence the viscosity and homogeneity of the sol, which are critical factors in forming uniform coatings on substrates. The concentration of ethanol can influence the microstructure of the silica gel. Higher ethanol content can lead to increased porosity and a more open network structure, which is beneficial for AR coatings as it can reduce the refractive index of the coating, enhancing its antireflective properties. Ethanol can also affect the kinetics of the sol-gel reactions. It can act as a medium for acid or base catalysts, which are often used to control the hydrolysis and condensation rates. The presence of ethanol can thus influence the size and distribution of silica particles, affecting the optical properties of the AR coating.

Ammonium hydroxide acts as catalysts that accelerate silicon alkoxides' hydrolysis and condensation reactions[102]. In a basic environment, the hydrolysis of the alkoxide groups is facilitated, leading to the formation of silanol groups (Si-OH). These groups then undergo condensation to form siloxane bonds (Si-O-Si), which are crucial for building the silica network[101].Base-catalysed sol-gel processes generally result in gels with a coarser texture compared to those formed under acidic conditions[103].

In addition, base ammonium hydroxide act as catalysts that accelerate the hydrolysis and condensation reactions of silicon alkoxides. In a basic environment, the

hydrolysis of the alkoxide groups is facilitated, leading to the formation of Si-OH. These groups then undergo condensation to form Si-O-Si bonds, which are crucial for building the silica network. Base-catalysed sol-gel processes generally result in gels with a coarser texture compared to those formed under acidic conditions.

At elevated temperatures, the polycondensation reaction among siliceous micelles is enhanced, forming denser silica shells and contributing to uniform particle sizes. As the temperature increases, the viscosity of the sol decreases, which can lead to faster solvent evaporation.

Water is essential for the hydrolysis of silicon alkoxide precursors, such as TEOS. During hydrolysis, water reacts with the alkoxide groups to form silanol groups (Si-OH) and alcohol by-products [79]. This step is critical for initiating the sol-gel process and forming the silica network. The concentration of water affects the condensation kinetics, which is the subsequent step after hydrolysis. Higher water concentrations can lead to increased porosity and lower connectivity in the resulting gel, as water molecules do not act as catalysts for the condensation reaction. Instead, they can slow down the condensation kinetics by increasing the average distance between reactive silanol groups, thus reducing the frequency of condensation reactions. However, excess of water can result in a more porous gel structure due to the dilution effect. This increased porosity can be beneficial for AR coatings, as it can lower the refractive index of the coating, enhancing its anti-reflective properties.

Ageing in the silica sol-gel process significantly affects the properties and performance of AR coatings. With increased sol ageing time, more oversized pores, larger than 100 nm, can form in the silica coatings. These pores may act as scattering

centres, which can scatter visible light and lower the transmittance of the coatings. An optimal ageing time is crucial to balance pore formation and achieve maximum transmittance. For instance, an optimal ageing time of 1 day was found to yield silica coatings with a maximum transmittance of 99.2%, an 8% increase compared to bare glass.

Ageing can lead to increased coalescence or bonding between particles, strengthening the gel structure[104]. Refluxing involves heating the reaction mixture, which can accelerate the hydrolysis and condensation reactions[72]. This can lead to a more complete conversion of the silicon alkoxide precursors into silanol groups and subsequently into a silica network. The increased reaction rates can result in a more uniform gel structure, which is beneficial for producing high-quality AR coatings. As ammonia is removed, through refluxing, the pH decreases to around 7, which terminates particle growth and stabilizes the sol-gel structure. The decrease in pH upon ammonia removal stops further particle growth, which is crucial for achieving the desired size and properties of the sol-gel particles.

The pH level during the sol-gel process influences the porosity and surface area of the silica gel. At higher pH levels, the gel tends to have a lower surface area and smaller pore volume. As the pH decreases to neutral, the specific surface area and pore volume increase, which can enhance the anti-reflective properties by reducing the coating's refractive index.

4.2. Assessment of reflectance, transmittance and emissivity of SiO_2 coatings

4.2.1. Presentation of results:

The FTIR and UV-Vis-NIR spectrophotometer results of the fabricated coatings are presented in this study starting from the graph of the glass, which was used as a reference, then follows the graph of the porous silica coatings fabricated with the sol containing 0.25 g, 0.40 g and then 0.60 g of pluronic F127. For each trial three graphs are presented, starting with 1-layer, 2-layer and then 3-layers. The three graphs for each trial are then combined to assess the changes in transmittance and emissivity of the coatings. A close-up graph for each trial is also presented with transmittance and emissivity. Furthermore, to observe the difference in trials the final graphs presented show the combined graph for 1 layer for all the coatings trials, followed by a separate graph of transmittance and emissivity for all the 1-layer coatings.

The following Figure 20 shows a 1 mm thick soda lime glass substrate optical results that was used in this study. The graph shows the grey line T_g as the transmittance of the glass, the dotted black line T_{dif} as the diffuse transmittance of the graph, the green line R_g indicate reflectance of the glass, the dotted R_{dif} indicate the diffuse reflectance and the red line shows the emissivity of the glass**.**

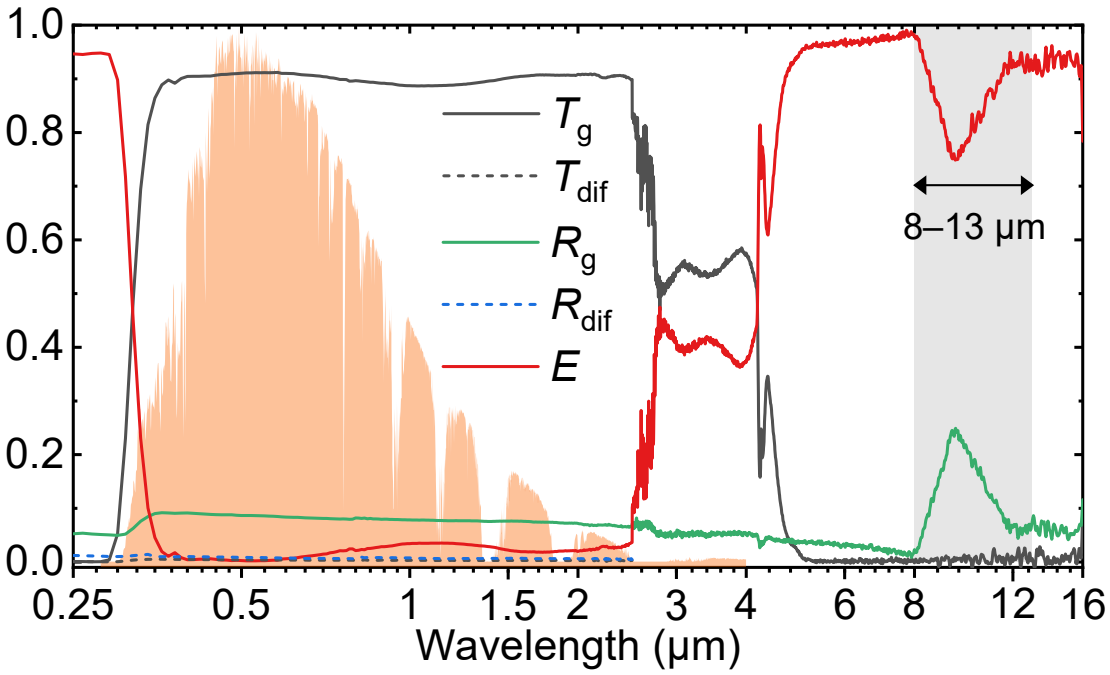

Figure 20 A 1 mm thick soda-lime glass substrate graph

Based on the results graph the transmittance of the glass at the solar spectrum in the range of 300 nm-1100nm is approximately 90%, this proves that there is a reflection loss of about 10% since not all the light has been transmitted. The 90% transmittance of the PV surface is also what is found in previous literature[27]. Furthermore, the emissivity of the glass is shown to be below 80% in the mid-infrared range (8-13μm). This means that there is a need to increase both the transmittance and emissivity of the glass substrate in Figure 20.

To improve the transmittance and emissivity of the glass in Figure 20, a silica sol that was prepared as indicated in Chapter 3 and was spin-coated on and sintered as shown in Chapter 3 of this study. The results for 1-layer porous silica coating prepared from a sol containing 0.25 g of pluronic F127 are as shown in Figure 21 -23.

The Figure 21 shows the graphical results of the 1-layer porous silica that was applied to a glass substrate with optical results in Figure 20. The graph shows the grey line T_g as the transmittance of the porous silica coatings, the dotted black line T_{dif} as the diffuse transmittance of the graph, the green line R_g indicate reflectance, the dotted R_{dif} indicate the diffuse reflectance and the red line shows the emissivity of the fabricated porous silica coatings.

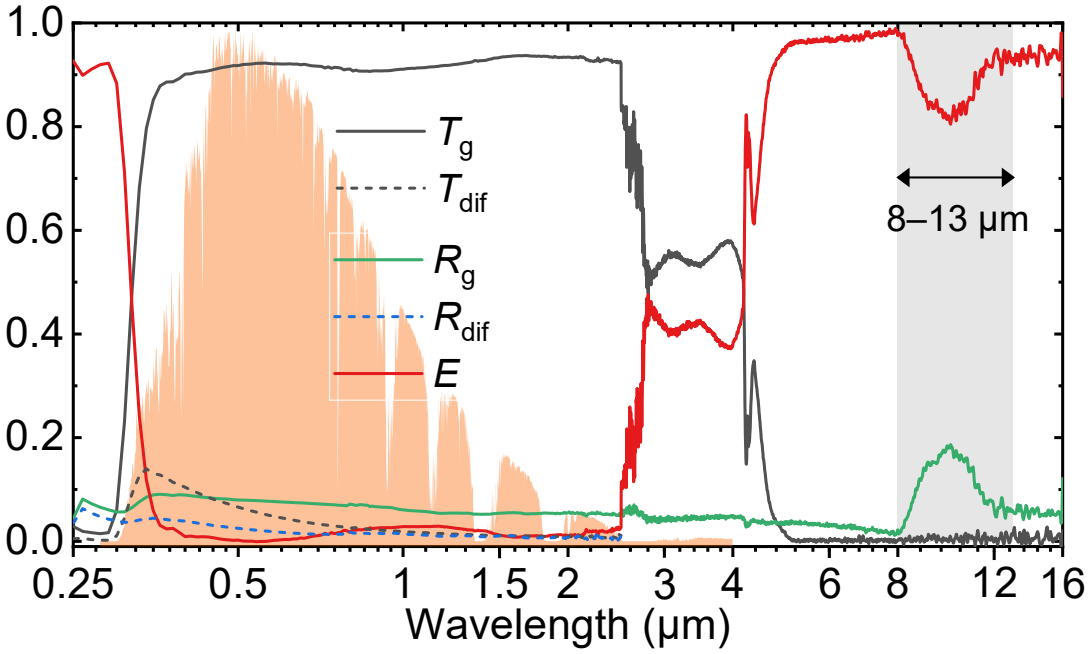

Figure 21 This graph shows the optical results for the 1- layers of porous silica coatings on glass with silica sol containing 0.25 g of PF-127

The optical results in Figure 21 of the 1-layer glass coated with porous silica (0.25 grams of PF-127) show an above 90% transmittance and around 81% emissivity compared to the glass substrate which means that the coating fabricated is anti-reflective and possess thermal emissivity properties.

To assess further, a second layer of porous silica coating was applied after about five minutes of air drying the first layer at room temperature. The graphical presentation of

the second layer porous silica coating optical results is shown in Figure 22. The graph (Fig.22) shows the grey line T_g as the transmittance of the porous silica coatings, the dotted black line T_{dif} as the diffuse transmittance of the graph, the green line R_g indicates reflectance, the dotted R_{dif} indicate the diffuse reflectance and the red line shows the emissivity of the fabricated porous silica coatings.

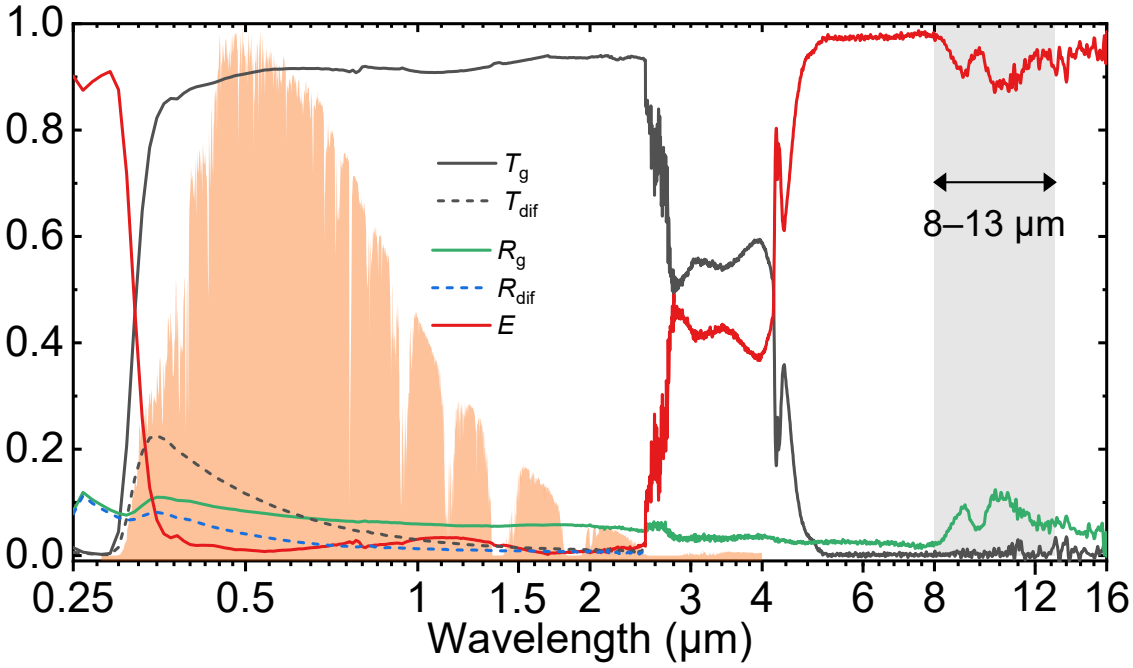

Figure 22 This graph shows the optical results for the 2 layers of porous silica coatings on glass with silica sol containing 0.25 g of PF-127

The graph in Figure 22 shows improvement of the coating in the emissivity going above 85% in the solar spectrum range 8-13μm. This shows that the thin film has radiative properties and can reduce the operating temperature of the solar module if applied to the surface of the solar PV panel. However, the transmittance of the 2 layers shows a reduction in transmittance in the solar spectrum range of 300-550 nm, with about 5% reduction in the solar spectrum of 300nm wavelength. This means that light energy with wavelengths of 300-400 nm is being scattered or absorbed

based on Beer Lambert law, and this could be due to the thickness that has increased. Since with an increase in layers, the thickness also increases.

To observe further improvements most especially in the solar spectrum range 8-13 μm a third layer was applied as indicated in this study, and the optical results are as shown below in figure 23. The graph (Figure 23) shows the grey line T_g as the transmittance of the porous silica coatings, the dotted black line T_{dif} as the diffuse transmittance of the graph, the green line R_g indicate reflectance, the dotted R_{dif} indicate the diffuse reflectance and the red line shows the emissivity of the fabricated porous silica coatings.

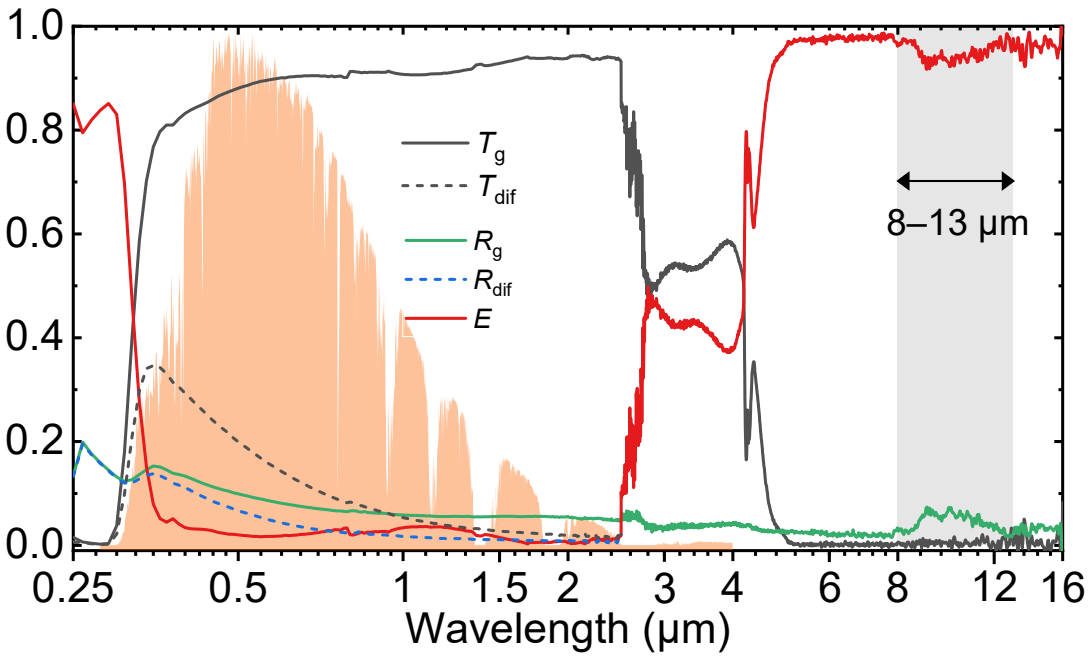

Figure 23 This graph shows the optical results for the 3 layers of porous silica coatings on glass with silica sol containing 0.25 g of PF-127

The graph clearly shows that there is an increase in emissivity of the fabricated coatings in comparison with the bare glass. This means that with an increase in layers

of porous silica coatings, the emissivity of the coating also increases. Furthermore, by observing a bare glass, 1 layer and 2 layers the emissivity increased from below 80% to above 90% in the 3 layers silica coatings. However, the transmittance declined from about 90% to 83 in the initial 300nm - 550 nm wavelength, which is due to the thickness of the coating fabricated[30].

To best analysed the fabricated coatings with the silica sol containing 0.25 g of PF-127 the graphs in figure 21 - 23 were combined using Origin Pro software for data analysis and the combined graphs are as shown in Figure 24 below. Figure 24 simply shows the transmittance, emissivity and reflectance with each coatings given a same colour.

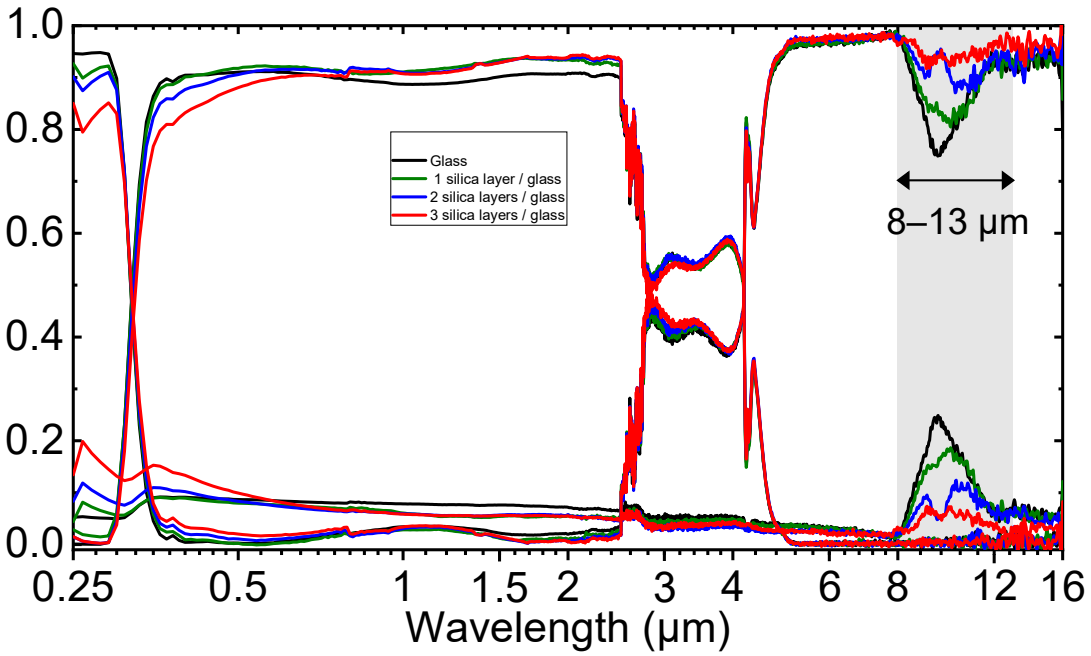

Figure 24 A comparison of 3 glass-coated porous silica layers (0.25 g PF127) with reference to the bare glass

It is observed that all the fabricated coatings have anti-reflective properties and however in the smaller wavelength between 300nm-700nm there seems to be high

reflectance or absorptance of light. To observe the results properly the graph of just transmittance and the other with just emissivity were drawn as shown in Figure 25, which is just a close-up view of the graph in Figure 24.

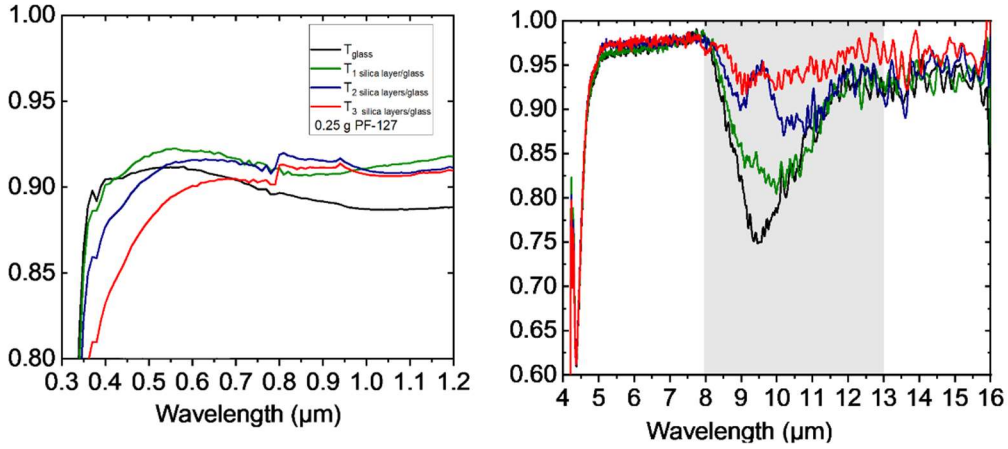

Figure 25 A comparison of 3 glass-coated porous silica layers (0.25g PF127) transmittance (left) and emissivity (right) with reference to the bare glass

Observing closely the Figure 25, it shows that the 1-layer coatings show better results in terms of transmittance in the solar spectrum range 300-110nm while the graph in Figure 25 (right) shows that the coatings with more layers of porous silica have much better emissivity readings compared to the bare glass, 1 layer and 2 layers.

To further improve the transmittance the silica sol with 0.40 g of PF-127 was prepared and sintered on a glass as shown earlier. Three coatings were fabricated, with 1 layer, 2 layers and 3 layers. The first graph in Figure 26 shows the optical results of 1-layer porous silica coatings prepared with silica sol containing 0.40 g of PF-127. The graph in Figure 26 shows the grey line T_g as the transmittance of the porous silica coatings, the dotted black line T_{dif} as the diffuse transmittance of the graph, the green line R_g indicate reflectance, the dotted R_{dif} indicate the diffuse

reflectance and the red line shows the emissivity of the fabricated porous silica coatings.

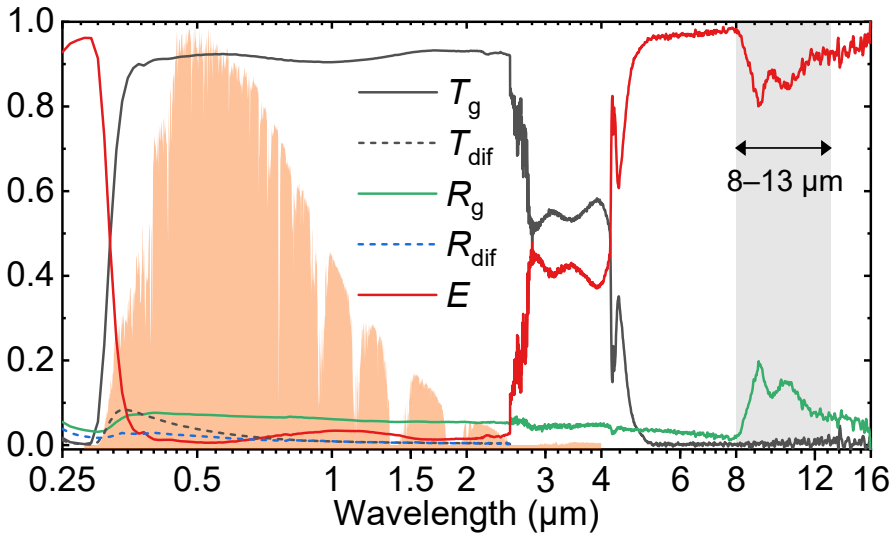

Figure 26 This graph shows the optical results for the 1 layer of porous silica coatings on glass with silica sol containing 0.40 g of PF-127

The graph in Figure 26 shows a significant improvement in transmittance from the smaller wavelength of 300nm to 1100nm of about a 2% increase, this means the increase in the amount of 0.40 might have worked in increasing the transmittance of light in the lower wavelength. The figure also shows that emissivity of about 81% although not so significant, it is above 80% compared to the bare glass substrate which is below 80%.

A porous silica coating with 2-layers was also fabricated from a silica sol containing 0.40 g pluronic F127. The optical results were presented as shown in Figure 27.

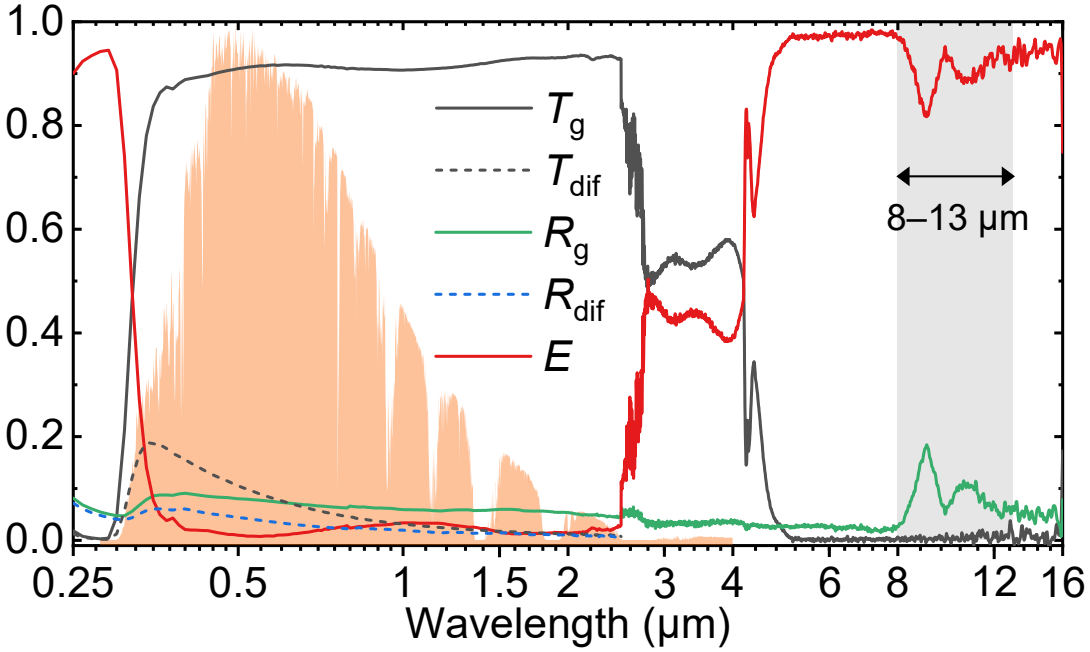

Figure 27 This graph shows the optical results for the 2 layer of porous silica coatings on glass with silica sol containing 0.40 g of PF-127

The 2-layers porous silica coatings in Figure 27 optical results show a slight decrease in transmittance at the lower wavelength between 300nm-550nm although still shows anti-reflect properties. With regards to the emissivity of the 2-layer coatings in Figure 27, the is not much noticeable change as the emissivity still looks like the one in figure 26. The emissivity results could be a most similar or with little change due to increase in porosity of the coatings, which means that the more the coatings become porous the less the coatings emit mid-infrared radiation.

To further observe the improvement in emissivity and transmittance, a 3 -layer coating was fabricated, and its optical results are as presented graphically in Figure 28. The graph in Figure 28 shows the grey line (T_g) as the transmittance of the porous silica coatings, the dotted grey line (T_{dif}) as the diffuse transmittance of the graph, the green

line (R_g) indicate reflectance, the dotted (R_{dif}) indicate the diffuse reflectance and the red line shows the emissivity (E)of the fabricated porous silica coatings**.**

To further observe the improvement in emissivity and transmittance, a 3-layers coating was fabricated, and its optical results are as presented graphically in Figure 28.

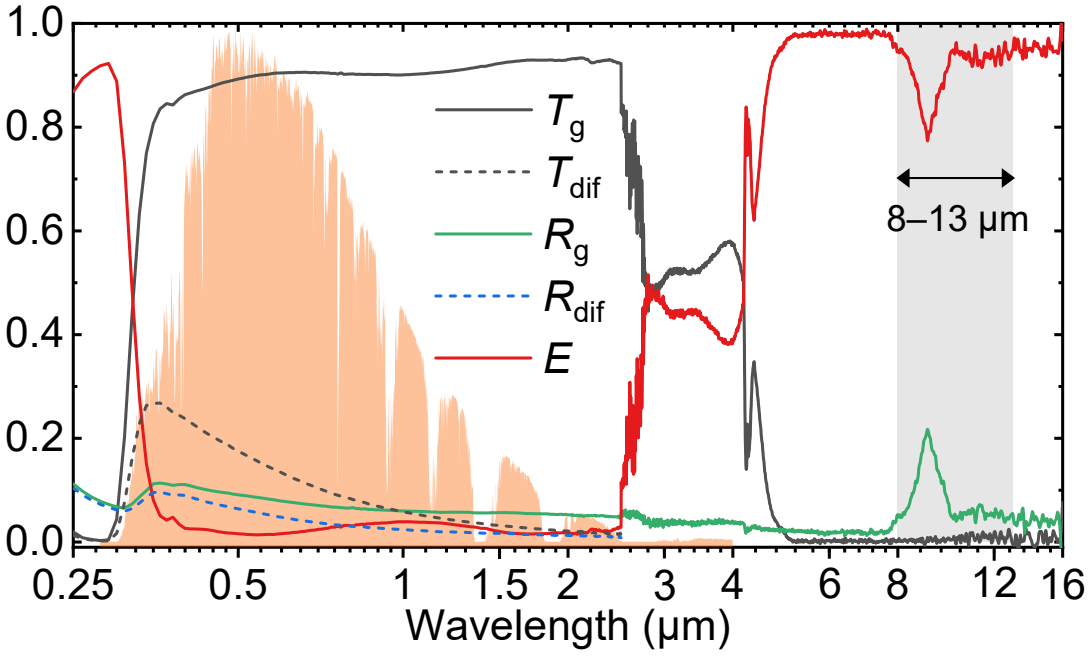

Figure 28 This graph shows the optical results for the 3 layer of porous silica coatings on glass with silica sol containing 0.40 g of PF-127

The Figure 28 shows the decline in the lower wavelength solar spectrum with 300 nm wavelength showing about a 6% decline in transmittance compared to a glass substrate which is at about 90% at the 300nm wavelength in the range of 300 nm to 1100nm.

The results for bare glass, 1-layer, 2-layers and 3-layers were also combined graphically to easily assess the variation. It was observed that the 1-layer showed much better results with lower wavelengths of 300nm until 1100nm wavelengths, and their transmittance of the coating is observed to be constantly above that of the

glass substrate, this is seen in Figure 30. The graph of the fabricated porous silica coatings with the silica sol containing 0.40 g of PF-127 as shown in Figure 26 -28, were combined using Origin Pro software for data analysis, yielding a combined graphs are as shown in figure 29 below. Figure 29 shows the transmittance, emissivity and reflectance with each coating given the same colour for each thin film.

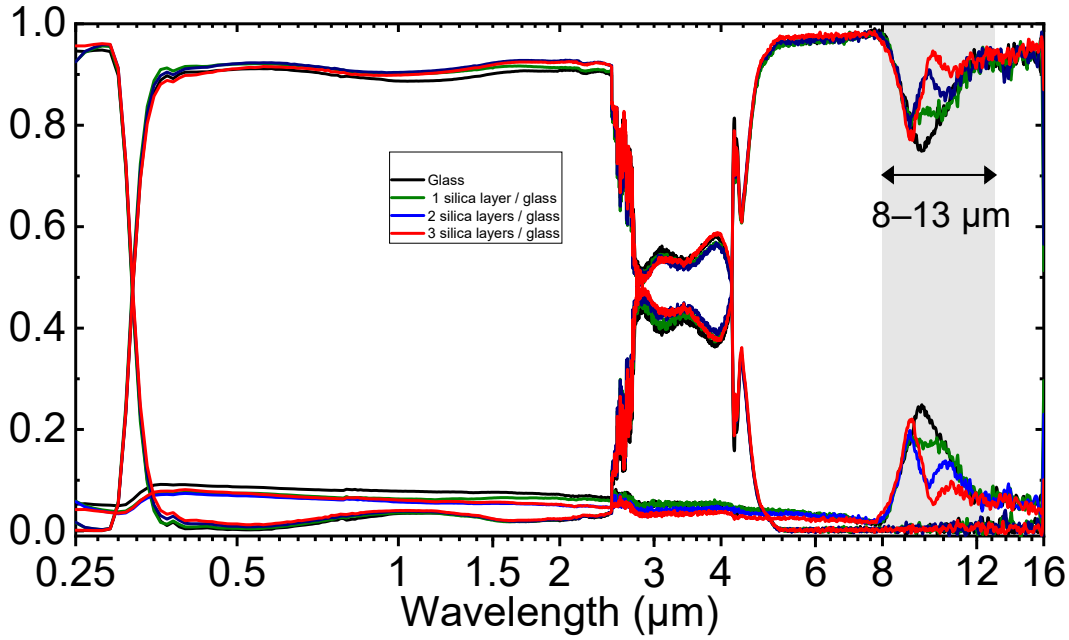

Figure 29 A comparison of 3 glass-coated porous silica layers (0.40 g PF127) with reference to the bare glass

To observe the results properly the graph of transmittance and emissivity were drawn separately as shown in Figure 30, which is just a close-up view of the graph in Figure 29. By observing the graph on transmittance, the two porous silica coatings lines, one with 1-layer and 2-layers are all above the line of the glass substrate as from the lower wavelength of 300nm-550nm, while the 3-layers line graph went just a bit below the graph of the glass at the 300nm-400nm wavelengths, this proves the silica sol of 0.40 g PF127 to be much more effective compare to the previous silica sol containing 0.25

g PF127. The graph of the transmittance of the combined graph of porous silica coatings containing 0.40 g of PF127 is as shown in the Figure 30 below.

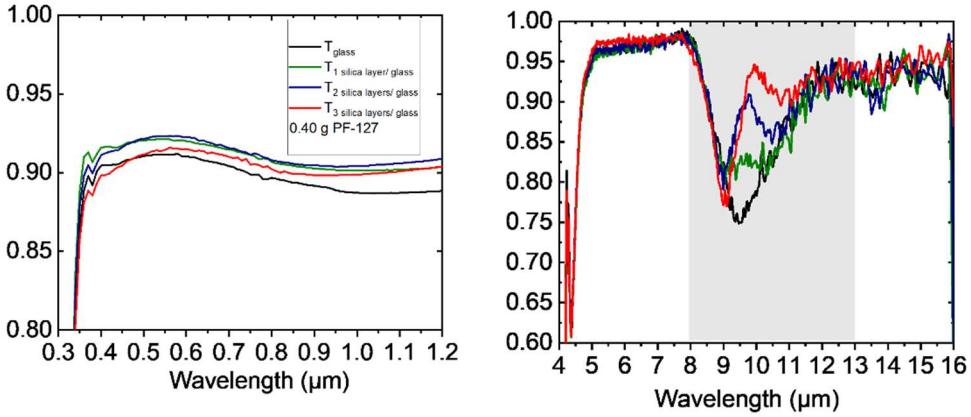

Figure 30 A comparison of 3 glass-coated porous silica layers (0.40g PF127) transmittance (left) and emissivity (right) with reference to the bare glass

On the other hand, the comparison of the 3-porous silica layers fabricated with silica containing 0.40 g of PF127 is as shown in Figure 30(left), with the colour and legend used the same as in Figure 30 (right). The emissivity in Figure 30 above, with the increase in porous silica layers, the emissivity tends to increase at the wavelength between 8.5-9.5 μm.

To further assess the porous silica coating the third trial was conducted with a silica sol containing 0.60 g of Pluronic F127, the fabricated coatings were prepared as indicated in Chapter 3 of this document and the optical results were analysed as shown in Figure 31, 32 and figure 33.

The 1-layer porous silica coatings with a silica sol containing 0.60 g of pluronic F127 are presented in the graph shown in Figure 31. The graph in Figure 31 shows the grey line T_g as the transmittance of the porous silica coatings, the dotted grey line T_{dif} as the diffuse transmittance of the graph, the green line R_g indicate reflectance, the dotted

R_{dif} indicate the diffuse reflectance and the red line E shows the emissivity of the fabricated porous silica coatings.

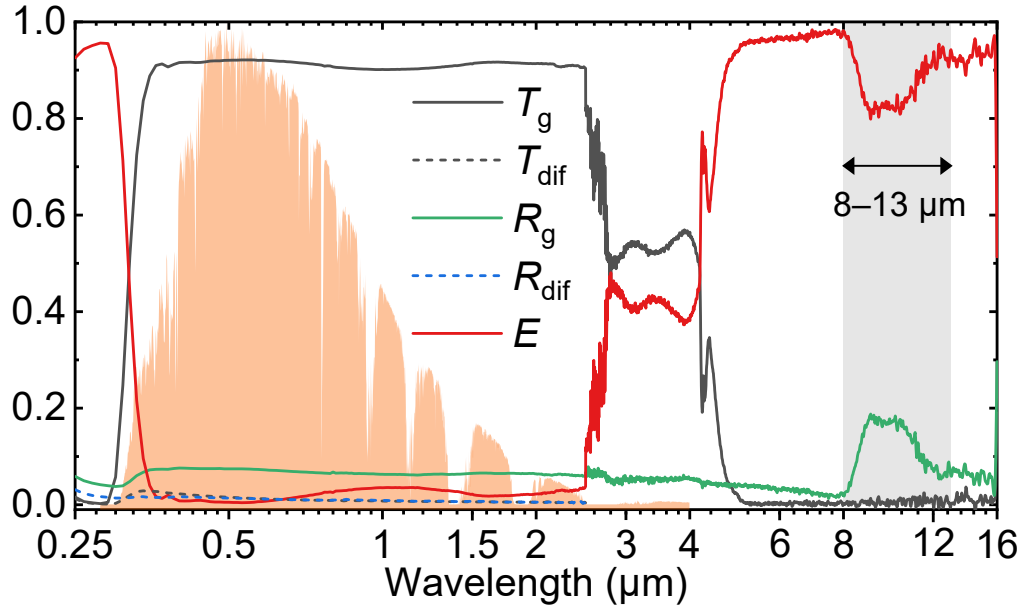

Figure 31 This graph shows the optical results for the 1 layer of porous silica coatings on glass with silica sol containing 0.60 g of PF-127

The 1-layer graph in Figure 31 shows the coating fabricated has transmittance slightly above 90% in the solar spectrum range of 300nm-1100nm, indicating that the coating has anti-reflection properties which means that optical loss due to reflectance can slightly be minimised by this coating. In addition, the emissivity of the fabricated porous silica coatings has emissivity slightly above 80% with about 2.5% in the mid-infrared range of 8-13μm.

Results of 2-layers of porous silica coatings with a silica sol containing 0.60 gm were also fabricated analysed and presented graphically as shown in Figure 36.

The graph in Figure 32 shows the grey line T_g as the transmittance of the porous silica coatings, the dotted grey line T_{dif} as the diffuse transmittance of the graph, the green line R_g indicate reflectance, the dotted R_{dif} indicate the diffuse reflectance and the red line E shows the emissivity of the fabricated porous silica coatings.

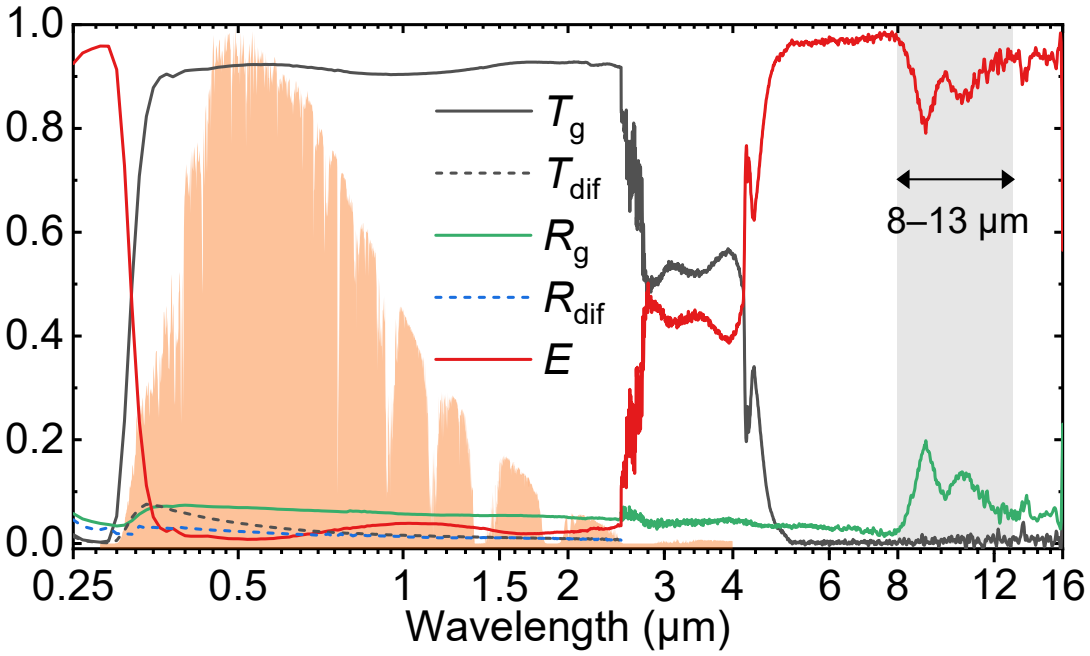

Figure 32 This graph shows the optical results for the 2 layers of porous silica coatings on glass with silica sol containing 0.60 g of PF-127

The 2-layer results presented in Figure 32 show a slight decline transmittance in transmittance and an observable increase in emissivity which is above 80% although there is a thinner sharp tail-like structure between 8.5 to 9.5 μm with about 85 % improvement between 9,5 and 13 μm.

To further investigate the results the 3-layers of porous silica coatings were obtained and presented as shown in Figure 33. The graph in Figure 31 shows the grey line T_g as the transmittance of the porous silica coatings, the dotted grey line T_{dif} as the

diffuse transmittance of the graph, the green line R_g indicates reflectance, the dotted R_{dif} indicate the diffuse reflectance and the red line E shows the emissivity of the fabricated porous silica coatings.

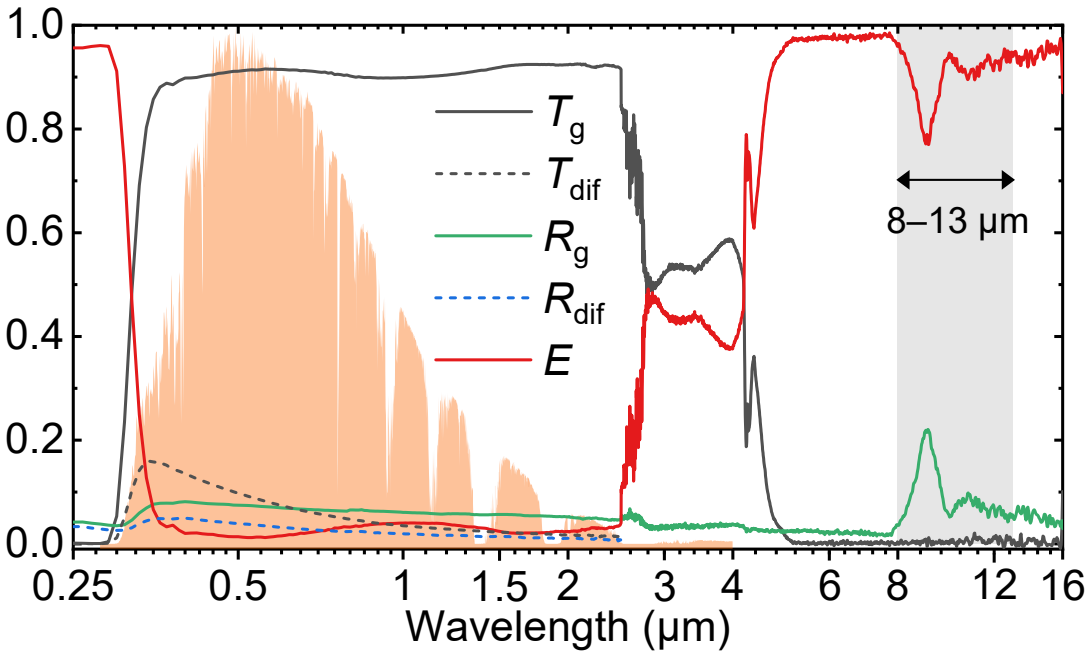

Figure 33 This graph shows the optical results for the 1 layer of porous silica coatings on glass with silica sol containing 0.60 g of PF-127

The 3-layer porous silica coatings results presented in Figure 33 show an approximately 3% decline in transmittance at 300 nm wavelength and an observable increase in emissivity which is above 80% although there is a thinner sharp-like structure between 8.5 to 9.5 μm decline in emissivity, with about 90 % improvement between 9,5 and 13 μm.

The results for bare glass and the porous silica coatings with 1-layer, 2-layers, and 3-layers, which were fabricated using a silica sol containing 0.60g of pluronic F127, were combined graphically for easier comparison. It was observed that the 1-layer and

2-layer coatings achieved significantly better results in terms of transmittance at lower wavelengths, ranging from 300 nm to 1100 nm, compared to the glass substrate and the 3-layer coating. The transmittance of both the 1-layer and 2-layer porous silica coatings consistently exceeded that of the glass substrate, as illustrated in Figures 31,32 and 33. Figure 34 displays the transmittance, emissivity, and reflectance for each fabricated coating containing 0.60g of PF-127 silica sol, with each coating represented in the same colour.

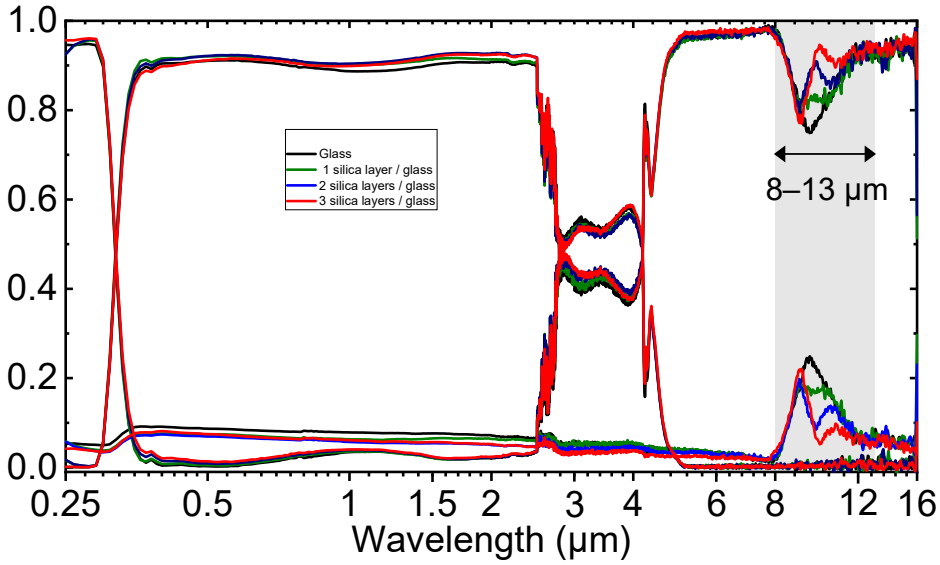

Figure 34 Comparison of 3 glass-coated porous silica layers (0.60 g PF127) with reference to the bare glass

It is clear that all the fabricated coatings exhibit anti-reflective properties; however, in the shorter wavelength range of 300 nm to 450 nm, there is a slight reflectance or absorptance of light for the three-layer porous silica coatings, which drop about 3% below the glass substrate. This phenomenon can be attributed to the increased thickness of the porous silica coatings. To analyse the results more effectively, graphs depicting transmittance and emissivity were created, as shown in Figure 35

respectively. These graphs below provide a closer view of the data presented in Figure 34.

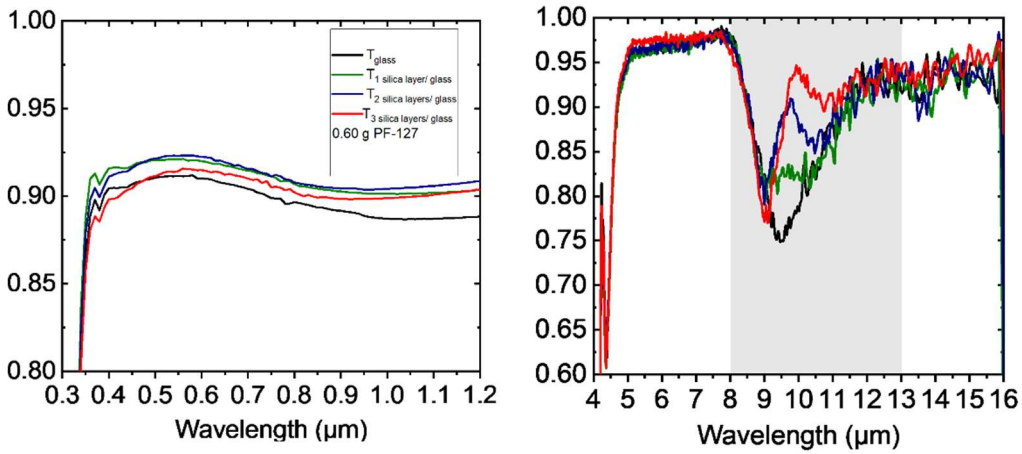

Figure 35 A Comparison of 3 glass-coated porous silica layers (0.60g PF127) transmittance (left) and emissivity (right) with reference to the bare glass

The close-up view of Figure 35 emissivity at the mid-infrared range 8-13μm was also obtained and presented. The legend and colour are as seen in Figure 35 (left).

The emissivity depicted in Figure 35 shows that as the number of porous silica layers increases, the emissivity tends to rise within the wavelength range of 9.5 to 13 micrometres. However, a decline in emissivity can be observed between 8.5 and 9.5 micrometres. This decrease may be attributed to the fact that a further increase in porosity reduces the vibrations that can emit mid-infrared radiation within the wavelength of 9 micrometres.

Since the transmittance of light in solar PV systems is crucial, the study found that a one-layer porous silica coating performs significantly better than both two-layer and three-layer coatings. The results from the one-layer porous silica coatings are combined, as shown in Figure 36, with a close view of transmittance and emissivity

shown in Figures 37, for better comparison across both the UV-Vis-NIR (300 nm - 1100 nm) and the mid-infrared (8-13 µm) ranges. To facilitate the observation of transmittance, emissivity, and reflectance, each coating is represented by the same colour. For a clearer understanding, references can be made to other graphs in this study, particularly Figure 16.

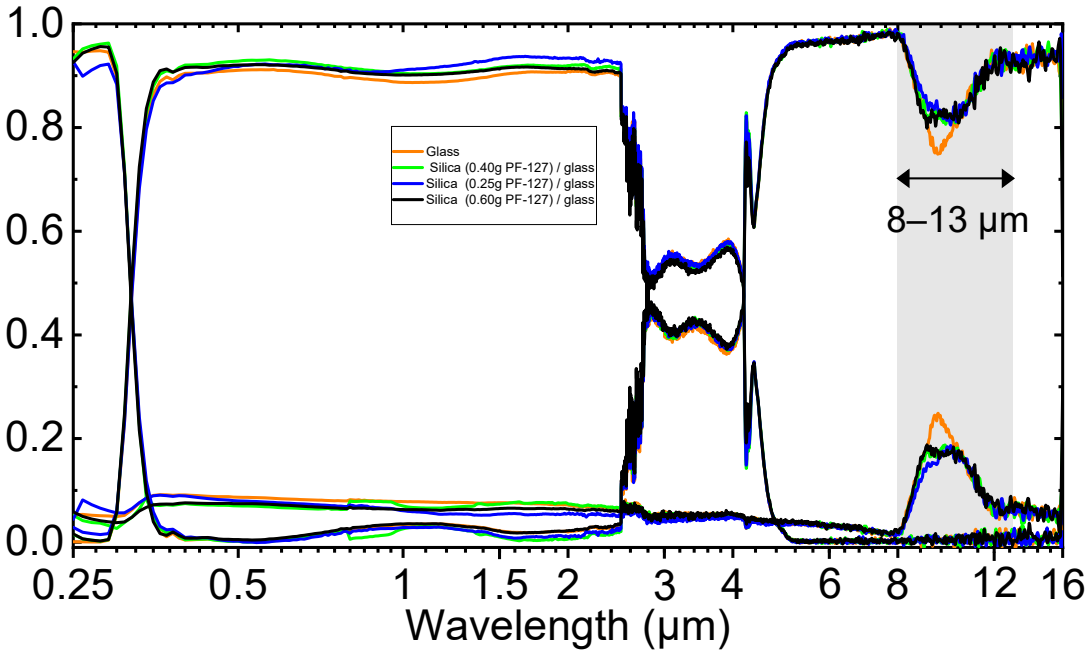

Figure 36 Comparison of 3 glass-coated porous silica 1 layer with reference to the glass

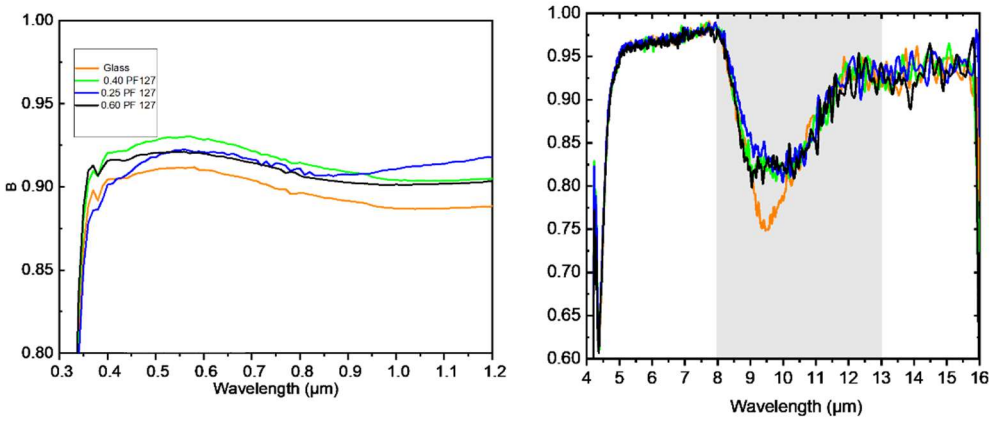

Figure 37 A comparison of 3 glass-coated porous silica 1 layer transmittance (left) and emissivity (right) with reference to the glass

The results from the combined graphs in Figures 37 of one layer demonstrate that the coatings exhibit anti-reflective properties, which is the primary objective of this study: to create a coating that enhances photovoltaic efficiency by increasing transmittance. In simpler terms, the coatings need to be anti-reflective.

The findings indicate a significant improvement in transmittance, particularly in the near-visible spectrum range of 300-550 nm, for both solutions with 0.40 and 0.60 grams of PF127. This suggests that reducing the amount of PF127 in the templating agents may lead to a decrease in transmittance.

To summarise, the most critical aspect of the study was assessing the emissivity and transmittance of the fabricated coatings to determine which coating performed best. Observing the transmittance of the fabricated coatings there is a decrease in transmittance with increase in thickness, with thickness between 200 nm- 1300nm in this study, in the previous study the thickness is ranging between 80 nm-200 nm showing high transmittance above 94%[51], [105]. The 1-layer porous silica coatings demonstrated the best transmittance results compared to the 2-layer and 3-layer porous silica coatings on glass. Among the 1-layer coatings, the porous silica coating prepared with silica sol containing 0.40 g of Pluronic F127 achieved the highest transmittance, approximately 93%, within the solar spectrum range of 300-1100 nm.

However, the emissivity of all the 1-layer porous silica coatings exceeded 80%, showing an improvement compared to the bare glass, which had an emissivity of 74%. This represents a 7% improvement, as seen in Figure 37. Furthermore, the coating with the highest emissivity in this study was the 3-layer coating manufactured from a silica sol containing 0.25 g of Pluronic F127. This coating achieved 93% emissivity for mid-

infrared radiation, reflecting an approximate 20% improvement over the glass substrate used.

Although the emissivity's of all three-layer porous silica coatings are notably high, their thickness can significantly impact the transmittance of light, particularly for wavelengths between 300 and 1100 nm. This effect is especially pronounced in the lower wavelength range of 300 to 550 nm. The study asserts that to evaluate the best coatings, it is essential to conduct further tests on actual PV surfaces coated with the porous silica layers developed in this research. This can be achieved by assessing the energy output of the solar PV panels.

The overall assessment is that the results proved how effective porous silica coatings is capable of emitting mid-infrared radiation to the cold universe. Although the topic is not over explored, with no specific related study on porous silica AR coating and radiative cooling, this study has proven potential of porous silica in cooling PV module to enhance its efficiency.

4.2.2. Discussion

The transmittance results indicate progressive fabrication of porous silica coatings which is anti-reflective and fit to be on the solar PV surface. The coatings fabricated is confirmed fit to be at the interface of the air and the glass as per the Fresnel's equations, this can be observed in figure 37, which shows the transmittance of the glass being around 90%, and about 2% lower than that of all the fabricated coatings. In previous study a single layer silica coating can obtain a 4-6% increase in transmittance above that of the glass depending on the wavelength interval of focus[51], [106]. Although the current study did not obtain the 4-6 % increase in transmittance this could be attributed to thickness which is 200nm and above while in the previous study the thickness was around 90 nm[51].

The highest emissivity obtained in this study is about 20 % with three layers and a thickness of about 1.135 μm. In comparison to the thickness of 90 nm in a study that obtained a transmittance of 99.4% at visible wavelengths from 380 nm to 800 nm it means the coating with highest emissivity is 12 times thicker than the coating observed in previous study with highest transmittance[51]. Therefore, for accurate measurements of the emissivity and transmittance of the coating a consistent thickness may be needed, however the study proves that the porous silica coating can be used for radiative cooling of solar PV, with the aim to increase their efficiency under high temperature environment.

4.3. Hydrophobicity of the fabricated coatings

4.3.1. Presentation of results:

The hydrophobicity of the coatings was not test it was rather assessed with water some few waters droplet (about 0.5 mL). Water droplets that are not attached firmly flat on the coating surface and can easily fall off typically exhibit hydrophobic properties, which is characteristic of hydrophobic surfaces this was observed as seen in Figure 38 (far left), the opposite coating on the far right in Figure 38 indicate hydrophilic properties. Hydrophobic surfaces have a contact angle greater than 90 degrees,

meaning water droplets form beads or spheres that barely touch the surface, making them easy to roll off[107].

Figure 38 Assessing the hydrophobicity of the fabricated porous silica coatings with the glass on the left and two porous silica-coated glass on the right

Figure 39 Porous silica-coated broken sample with hydrophobic properties

Based on the results observed, the glass in Figure 38 on the left shows hydrophobic behaviour, along with one of the broken samples. Since the broken porous silica-coated glass sample in Figure 39 obtains hydrophobic properties, it could be due to a longer exposer period in the HMDS since it was exposed 5 minutes longer than other samples, based on previous studies, the coatings contact angle increases with a longer immersion period in HMDS[108].

4.3.2. Discussions

Although HMDS did not produce hydrophobic coatings in this study, it did create them in a previous study, which found that the contact angle value obtained for the treatment in 40% HMDS solution for 15 min was above 80°, which was similar to the value obtained for 100% HMDS solution 5 min treatment.[13]. Although, the concentration of the HMDS solution used in this study was 99.9%, with the immersion time of 5 minutes this did not yield the same results, and this could be due to other unknown factors like heat treating time. HMDS is known not to have any effect on the thickness of the coating, but it tends to decrease transmittance, which may be attributed to an increase in the refractive index[13].

Chapter 5

Conclusion and Recommendations

This chapter presents a summary of the study, clearly defining its achievements and challenges and provides recommendations to other researchers, industries and future studies.

5.1 Conclusions

In conclusion, this study successfully applied the sol/gel method along with spin coating techniques to fabricate nine porous silica coatings. These coatings were designed to possess anti-reflection properties at the solar spectrum (300nm-1100nm) and high emissivity of mid-infrared radiation (8-13μm), which can reduce the operating temperature of solar photovoltaic modules and improve their efficiency. The study effectively achieved its objectives in creating these functional coatings.

The study obtained an increase in transmittance by 2 % relative to the solar spectrum range (visible range) for a single layer of coatings fabricated with a silica sol containing 0.60 g of pluronic F127. The study observed that as the layers of the coatings increases, the transmittance diminution in the 300nm -550nm range, and the emissivity tends to increase with more layers of the coatings and vice versa. It is also observed that as the amount of pluronic F127 increases the emissivity is affected, reducing, this shrinking can be observed as the initial emissivity in the three layers coatings of 0.25 g is way better than for 0.40 and 0.60 g, the reverse can be due to thickness of the coatings. The study achieved significance emissivity of about 19 %

relative, in the atmospheric window (8-13μm), for three layers of 0.25 g of Pluronic F127. With the increase in PF127, the transmittance improves at the range of 300 n them-550nm, indicating the increased porosity of the synthesised particles. The smallest thickness of the single layer achieved was observed with a scanning electron microscope to be around 200 nm. The smallest thickness of all 3 layers coatings fabricated is estimated to be around 959 nm mainly observed to be from porous coatings fabricated with more about of Pluronic F127 (0.60g). The lowest amount of silica sol containing Pluronic F127 obtaining the thicker 1-layer coatings of 754.5 nm. The thickness of the coatings fabricated in this study indicates that the silica sol used in this study has lower viscosity, leading to a thicker coating. In addition, the increase in spin speed could reduce the thickness of the fabricated coatings since much thinner coatings can be produced with higher spin speed[64]. These findings obtained in this study lay a strong foundation for porous silica and its importance in radiative cooling industries and not just as an anti-reflective coating for solar PV surface. The emissivity results obtained in this is of great importance the PV industries as works can be done in bringing both transmittance and emissivity to go above 95% if not 98%. The development in this study has a possibility of reducing the operating temperature of the solar PV and enhancing its efficiency, which is of great importance to PV system owner that are based in hot climate conditions.

Regarding the hydrophobicity of the coatings in this study, after immersing the coatings in the HMDS solution, the study did not observe the hydrophobicity of the coatings. This could be that the time of immersing the coating in HMDS longer time may be required to realise the hydrophobic the produce a coating with hydrophobic porous silica coatings. Furthermore, the hardness of the coatings was also observed,

although no testing was done. The coatings were observed to have good mechanical strength due to the acid catalysis that was used. In the making of the silica sol. Overall, the study achieved its objectives in fabricating anti-reflective coatings with radiative cooling properties that can enhance PV efficiency.

5.2 Recommendations

To enhance their hydrophobic properties by increasing the immersion time of the coatings in the HMDS solution or by using alternative methods such as chemical vapour deposition, to apply a hydrophobic layer. Additionally, there is a need to create smaller particles, which can be achieved by lowering the chemical reaction temperature. Smaller particles are recommended as they result in less light scattering than larger ones, thereby improving the transmittance of the coatings. The study recommends varying the spin speed to produce coatings with smaller thickness. The study recommends on producing a coating with moderate viscosity suitable for fabricating thinner coating with a spin coater. The study also recommends a pencil test to examine the hardness of the fabricated coatings.

Furthermore, the study suggests conducting outdoor tests on the fabricated coatings to measure and observe their radiative cooling effects in outdoor environment. It is also advisable to test different coatings on PV systems to evaluate the efficiency of various coating porosities, with the aim of identifying the optimal power output.

References

[1] F. Grubišić-Čabo, S. Nižetić, I. Marinić Kragić, and D. Čoko, "Further progress in the research of fin-based passive cooling technique for the free-standing silicon photovoltaic panels," *Int J Energy Res*, vol. 43, no. 8, pp. 3475–3495, Jun. 2019, Doi: 10.1002/er.4489.

[2] K. Hasan, S. B. Yousuf, M. S. H. K. Tushar, B. K. Das, P. Das, and M. S. Islam, "Effects of different environmental and operational factors on the PV performance: A comprehensive review," Feb. 01, 2022, *John Wiley and Sons Ltd*. Doi: 10.1002/ese3.1043.

[3] L. Angel *et al.*, "Efficiency and Sustainability in Solar Photovoltaic Systems: A Review of Key Factors and Innovative Technologies," *Eng 2025, Vol. 6, Page 50*, vol. 6, no. 3, p. 50, Mar. 2025, Doi: 10.3390/ENG6030050.

[4] M. A. Zahid, M. de Assis Rabelo, H. Yousuf, Y. Kim, D. P. Pham, and J. Yi, "Anti-reflective coating and cooling technique for innovative photovoltaic system in tropical region," *J Power Sources*, vol. 564, Apr. 2023, Doi: 10.1016/j.jpowsour.2023.232812.

[5] M. M. Rahman, M. Hasanuzzaman, and N. A. Rahim, "Effects of various parameters on PV-module power and efficiency," *Energy Convers Manag*, vol. 103, pp. 348–358, Jul. 2015, Doi: 10.1016/j.enconman.2015.06.067.

[6] A. M. Law, L. O. Jones, and J. M. Walls, “The performance and durability of Anti-reflection coatings for solar module cover glass – a review,” Sep. 01, 2023, *Elsevier Ltd*. Doi: 10.1016/j.solener.2023.06.009.

[7] A. M. Oni, A. S. M. Mohsin, M. M. Rahman, and M. B. Hossain Bhuian, “A comprehensive evaluation of solar cell technologies, associated loss mechanisms, and efficiency enhancement strategies for photovoltaic cells,” *Energy Reports*, vol. 11, pp. 3345–3366, Jun. 2024, Doi: 10.1016/J.EGYR.2024.03.007.

[8] M. Mussard and M. Amara, “Performance of solar photovoltaic modules under arid climatic conditions: A review,” *Solar Energy*, vol. 174, pp. 409–421, Nov. 2018, Doi: 10.1016/J.SOLENER.2018.08.071.

[9] A. Shukla, K. Kant, A. Sharma, and P. H. Biwole, “Cooling methodologies of photovoltaic module for enhancing electrical efficiency: A review,” *Solar Energy Materials and Solar Cells*, vol. 160, pp. 275–286, Feb. 2017, Doi: 10.1016/J.SOLMAT.2016.10.047.

[10] E. Skoplaki and J. A. Palyvos, “On the temperature dependence of photovoltaic module electrical performance: A review of efficiency/power correlations,” *Solar Energy*, vol. 83, no. 5, pp. 614–624, May 2009, Doi: 10.1016/j.solener.2008.10.008.

[11] H. K. Raut, V. A. Ganesh, A. S. Nair, and S. Ramakrishna, “Anti-reflective coatings: A critical, in-depth review,” Oct. 2011. Doi: 10.1039/c1ee01297e.

[12] A. M. Law, L. O. Jones, and J. M. Walls, “The performance and durability of Anti-reflection coatings for solar module cover glass – a review,” Sep. 01, 2023, *Elsevier Ltd*. Doi: 10.1016/j.solener.2023.06.009.

[13] G. San Vicente, R. Bayón, N. Germán, and A. Morales, “Surface modification of porous antireflective coatings for solar glass covers,” *Solar Energy*, vol. 85, no. 4, pp. 676–680, Apr. 2011, Doi: 10.1016/j.solener.2010.06.009.

[14] E. Zäll, S. Karlsson, M. Järn, J. Segervald, P. Lundberg, and T. Wågberg, “Durability of antireflective SiO2 coatings with closed pore structure,” *Solar Energy Materials and Solar Cells*, vol. 261, p. 112521, Oct. 2023, Doi: 10.1016/J.SOLMAT.2023.112521.

[15] S. M. Kiwan and A. M. Khlefat, “Thermal cooling of photovoltaic panels using porous material,” *Case Studies in Thermal Engineering*, vol. 24, Apr. 2021, Doi: 10.1016/j.csite.2020.100837.

[16] K. Alam *et al.*, “Antireflection, Superhydrophilic Nano-Porous SiO2 Coating based on Aerosol Impact Spray Deposition Technique for Solar PV Module,” *Coatings 2019, Vol. 9, Page 497*, vol. 9, no. 8, p. 497, Aug. 2019, Doi: 10.3390/COATINGS9080497.

[17] A. Vincent, S. Babu, E. Brinley, A. Karakoti, S. Deshpande, and S. Seal, “Role of catalyst on refractive index tunability of porous silica antireflective coatings by sol-gel technique,” *Journal of Physical Chemistry C*, vol. 111, no. 23, pp. 8291–8298, Jun. 2007, Doi: 10.1021/JP0700736.

[18] E. M. Björk, F. Söderlind, and M. Odén, “Tuning the shape of mesoporous silica particles by alterations in parameter space: From rods to platelets,” *Langmuir*, vol. 29, no. 44, pp. 13551–13561, Nov. 2013, Doi: 10.1021/LA403201V.

[19] S. Cai, Y. Zhang, H. Zhang, H. Yan, H. Lv, and B. Jiang, “Sol-gel preparation of hydrophobic silica antireflective coatings with low refractive index by base/acid two-step catalysis,” *ACS Appl Mater Interfaces*, vol. 6, no. 14, pp. 11470–11475, Jul. 2014, Doi: 10.1021/AM501972Y.

[20] A. Kumar and A. Chowdhury, “Effect of multilayer selective radiative anti-reflective coating on crystalline silicon photovoltaics for operating temperature reduction,” *International Journal of Sustainable Energy*, pp. 982–996, 2020, Doi: 10.1080/14786451.2020.1785466.

[21] Q. Hassan *et al.*, “The renewable energy role in the global energy Transformations,” *Renewable Energy Focus*, vol. 48, p. 100545, Mar. 2024, Doi: 10.1016/J.REF.2024.100545.

[22] P. A. Lynn, “Electricity from Sunlight: An Introduction to Photovoltaics,” *Electricity from Sunlight: An Introduction to Photovoltaics*, Apr. 2010, Doi: 10.1002/9780470710111.

[23] O. Ellabban, H. Abu-Rub, and F. Blaabjerg, “Renewable energy resources: Current status, future prospects and their enabling technology,” *Renewable and Sustainable Energy Reviews*, vol. 39, pp. 748–764, 2014, Doi: 10.1016/j.rser.2014.07.113.

[24] L. Hernández-Callejo, S. Gallardo-Saavedra, and V. Alonso-Gómez, “A review of photovoltaic systems: Design, operation and maintenance,” *Solar Energy*, vol. 188, pp. 426–440, Aug. 2019, Doi: 10.1016/J.SOLENER.2019.06.017.

[25] S. K. Nag, T. K. Gangopadhyay, and J. Paserba, “Solar Photovoltaics: A Brief History of Technologies [History],” *IEEE Power and Energy Magazine*, vol. 20, no. 3, pp. 77–85, 2022, Doi: 10.1109/MPE.2022.3150814.

[26] S. Sugianto, “Comparative Analysis of Solar Cell Efficiency between Monocrystalline and Polycrystalline,” *INTEK: Jurnal Penelitian*, vol. 7, no. 2, pp. 92–100, Dec. 2020, Doi: 10.31963/intek.v7i2.2625.

[27] B. L. Allsopp *et al.*, “Towards improved cover glasses for photovoltaic devices,” *Progress in Photovoltaics: Research and Applications*, vol. 28, no. 11, pp. 1187–1206, Nov. 2020, Doi: 10.1002/PIP.3334.

[28] X. D. He, K. E. Torrance, F. X. Sillion, and D. P. Greenberg, “A comprehensive physical model for light reflection,” *ACM SIGGRAPH Computer Graphics*, vol. 25, no. 4, pp. 175–186, Jul. 1991, Doi: 10.1145/127719.122738.

[29] R. G. Newton, “Scattering Theory of Waves and Particles,” *Scattering Theory of Waves and Particles*, 1982, Doi: 10.1007/978-3-642-88128-2.

[30] N. Shanmugam, R. Pugazhendhi, R. M. Elavarasan, P. Kasiviswanathan, and N. Das, “Anti-reflective coating materials: A holistic review from PV

perspective," *Energies (Basel)*, vol. 13, no. 10, May 2020, Doi: 10.3390/en13102631.

[31] J. Siecker, K. Kusakana, and B. P. Numbi, "A review of solar photovoltaic systems cooling technologies," *Renewable and Sustainable Energy Reviews*, vol. 79, pp. 192–203, Nov. 2017, Doi: 10.1016/J.RSER.2017.05.053.

[32] M. Chen, D. Pang, X. Chen, H. Yan, and Y. Yang, "Passive daytime radiative cooling: Fundamentals, material designs, and applications," *EcoMat*, vol. 4, no. 1, p. e12153, Jan. 2022, Doi: 10.1002/EOM2.12153.

[33] Z. Peng, M. R. Herfatmanesh, and Y. Liu, "Cooled solar PV panels for output energy efficiency optimisation," *Energy Convers Manag*, vol. 150, pp. 949–955, Oct. 2017, Doi: 10.1016/J.ENCONMAN.2017.07.007.

[34] M. Sharaf, M. S. Yousef, and A. S. Huzayyin, "Review of cooling techniques used to enhance the efficiency of photovoltaic power systems," Apr. 01, 2022, *Springer Science and Business Media Deutschland GmbH*. Doi: 10.1007/s11356-022-18719-9.

[35] E. Akerboom, T. Veeken, C. Hecker, J. Van De Groep, and A. Polman, "Passive Radiative Cooling of Silicon Solar Modules with Photonic Silica Microcylinders," *ACS Photonics*, vol. 9, no. 12, pp. 3831–3840, Dec. 2022, Doi: 10.1021/acsphotonics.2c01389.

[36] W. Li, Y. Shi, K. Chen, L. Zhu, and S. Fan, "A Comprehensive Photonic Approach for Solar Cell Cooling," *ACS Photonics*, vol. 4, no. 4, pp. 774–782, Apr. 2017, Doi: 10.1021/acsphotonics.7b00089.

[37] T. Wang, Y. Wu, L. Shi, X. Hu, M. Chen, and L. Wu, “A structural polymer for highly efficient all-day passive radiative cooling,” *Nat Commun*, vol. 12, no. 1, Dec. 2021, Doi: 10.1038/s41467-020-20646-7.

[38] N. Shanmugam, R. Pugazhendhi, R. M. Elavarasan, P. Kasiviswanathan, and N. Das, “Anti-reflective coating materials: A holistic review from PV perspective,” *Energies (Basel)*, vol. 13, no. 10, May 2020, Doi: 10.3390/en13102631.

[39] R. A. Messenger and A. Abtahi, “Photovoltaic Systems Engineering,” *Photovoltaic Systems Engineering*, Sep. 2018, Doi: 10.1201/9781315218397.

[40] A. Kumar and A. Chowdhury, “Effect of multilayer selective radiative anti-reflective coating on crystalline silicon photovoltaics for operating temperature reduction,” *International Journal of Sustainable Energy*, pp. 982–996, 2020, Doi: 10.1080/14786451.2020.1785466.

[41] X. Cui *et al.*, “A hydrophobic and abrasion-resistant MgF2 coating with an ultralow refractive index for double-layer broadband antireflective coatings,” *J Mater Chem C Mater*, vol. 5, no. 12, pp. 3088–3096, Mar. 2017, Doi: 10.1039/C6TC05307F.

[42] W. Xie, T. Aubert, Z. Hens, S. Verstuyft, Y. Zhu, and D. Van Thourhout, “Low-loss silicon nitride waveguide hybridly integrated with colloidal quantum dots,” *Optics Express, Vol. 23, Issue 9, pp. 12152-12160*, vol. 23, no. 9, pp. 12152–12160, May 2015, Doi: 10.1364/OE.23.012152.

[43] M. Szindler and M. Szindler, “Application of Al2O3, ZnO, and TiO_2 ALD thin films as antireflection coating in the silicon solar cells,” *Opto-Electronics Review*, vol. 31, no. 4, 2023, Doi: 10.24425/opelre.2023.148223.

[44] N. Shanmugam, R. Pugazhendhi, R. M. Elavarasan, P. Kasiviswanathan, and N. Das, “Anti-Reflective Coating Materials: A Holistic Review from PV Perspective,” *Energies 2020, Vol. 13, Page 2631*, vol. 13, no. 10, p. 2631, May 2020, Doi: 10.3390/EN13102631.

[45] B. Yao, X. Hu, J. Liu, K. Chen, and J. Liu, “Preparation and properties of high refractive index ZrO2 nano-hybrid materials,” *Mater Lett*, vol. 261, Feb. 2020, Doi: 10.1016/j.matlet.2019.126878.

[46] S. Maqsood *et al.*, “Assessment of different optimized anti-reflection coatings for ZnO/Si heterojunction solar cells,” *Ceram Int*, vol. 49, no. 23, pp. 37118–37126, Dec. 2023, Doi: 10.1016/j.ceramint.2023.08.313.

[47] M. M. Hawkeye, M. T. Taschuk, and M. J. Brett, “Glancing Angle Deposition of Thin Films: Engineering the Nanoscale,” *Glancing Angle Deposition of Thin Films: Engineering the Nanoscale*, pp. 1–299, Oct. 2014, Doi: 10.1002/9781118847510.

[48] A. B. D. Nandiyanto, N. Hagura, F. Iskandar, and K. Okuyama, “Design of a highly ordered and uniform porous structure with multisized pores in film and particle forms using a template-driven self-assembly technique,” *Acta Mater*, vol. 58, no. 1, pp. 282–289, Jan. 2010, Doi: 10.1016/J.ACTAMAT.2009.09.004.

[49] K. V. Baryshnikova, M. I. Petrov, V. E. Babicheva, and P. A. Belov, "Plasmonic and silicon spherical nanoparticle antireflective coatings," *Scientific Reports 2016 6:1*, vol. 6, no. 1, pp. 1–11, Mar. 2016, Doi: 10.1038/srep22136.

[50] Y. Hewakuruppu, R. A. Taylor, D. DeJarnette, and T. P. Otanicar, "Filtering light with nanoparticles: a review of optically selective particles and applications," *Advances in Optics and Photonics, Vol. 8, Issue 3, pp. 541-585*, vol. 8, no. 3, pp. 541–585, Sep. 2016, Doi: 10.1364/AOP.8.000541.

[51] J. Chen *et al.*, "A facile strategy to prepare antireflection coatings with high transmittance and improved mechanical stability and application in crystalline silicon solar modules," *J Solgel Sci Technol*, vol. 103, no. 2, pp. 360–366, Aug. 2022, Doi: 10.1007/s10971-022-05790-4.

[52] L. P. Singh *et al.*, "Sol-Gel processing of silica nanoparticles and their applications," 2014, *Elsevier B.V.* Doi: 10.1016/j.cis.2014.10.007.

[53] A. E. Danks, S. R. Hall, and Z. Schnepp, "The evolution of 'sol–gel' chemistry as a technique for materials synthesis," *Mater Horiz*, vol. 3, no. 2, pp. 91–112, Feb. 2016, Doi: 10.1039/C5MH00260E.

[54] S. Esposito, "'Traditional' sol-gel chemistry as a powerful tool for the preparation of supported metal and metal oxide catalysts," Feb. 23, 2019, *MDPI AG*. Doi: 10.3390/ma12040668.

[55] D. Bokov *et al.*, "Nanomaterial by Sol-Gel Method: Synthesis and Application," 2021, *Hindawi Limited*. Doi: 10.1155/2021/5102014.

[56] L. C. Klein and R. H. Woodman, “Porous silica by the sol-gel process,” *Key Eng Mater*, vol. 115, pp. 109–124, 1996, Doi: 10.4028/www.scientific.net/kem.115.109.

[57] M. L. Zheludkevich, I. M. Salvado, and M. G. S. Ferreira, “Sol–gel coatings for corrosion protection of metals,” *J Mater Chem*, vol. 15, no. 48, pp. 5099–5111, Dec. 2005, Doi: 10.1039/B419153F.

[58] C. A. Milea, C. Bogatu, and A. Duta, “The Influence of Parameters in Silica Sol- Gel Process,” *Bulletin of the Transilvania University of Brasov. Series I - Engineering Sciences*, vol. 4, no. 53, pp. 59–66, Jul. 2011, Accessed: Apr. 17, 2025. [Online]. Available: https://webbut.unitbv.ro/index.php/Series_I/article/view/6140

[59] T. I. Awan, S. Afsheen, and S. Kausar, “Chemical Vapor Deposition Technique,” *Thin Film Deposition Techniques*, pp. 65–96, 2025, Doi: 10.1007/978-981-96-1364-9_3.

[60] K. L. Choy, “Chemical vapour deposition of coatings,” *Prog Mater Sci*, vol. 48, no. 2, pp. 57–170, Jan. 2003, Doi: 10.1016/S0079-6425(01)00009-3.

[61] C. Li *et al.*, “Electrochemical Deposition: An Advanced Approach for Templated Synthesis of Nanoporous Metal Architectures,” *Acc Chem Res*, vol. 51, no. 8, pp. 1764–1773, Aug. 2018, Doi: 10.1021/ACS.ACCOUNTS.8B00119.

[62] S. M. Rossnagel, “Thin film deposition with physical vapor deposition and related technologies,” *Journal of Vacuum Science & Technology A*, vol. 21, no. 5, pp. S74–S87, Sep. 2003, Doi: 10.1116/1.1600450.

[63] A. Baptista, F. Silva, J. Porteiro, J. Míguez, and G. Pinto, “Sputtering Physical Vapour Deposition (PVD) Coatings: A Critical Review on Process Improvement and Market Trend Demands,” *Coatings 2018, Vol. 8, Page 402*, vol. 8, no. 11, p. 402, Nov. 2018, Doi: 10.3390/COATINGS8110402.

[64] H. Soonmin, “Thin film deposited by spin coating technique: review,” *J. Chem*, vol. 11, no. 4, pp. 38–47, 2021, Doi: 10.15228/2021.v11.i03-4.p07.

[65] M. Faustini, B. Louis, P. A. Albouy, M. Kuemmel, and D. Grosso, “Preparation of sol-gel films by dip-coating in extreme conditions,” *Journal of Physical Chemistry C*, vol. 114, no. 17, pp. 7637–7645, May 2010, Doi: 10.1021/jp9114755.

[66] L. E. Scriven, “Physics and Applications of DIP Coating and Spin Coating,” *MRS Proceedings*, vol. 121, no. 1, pp. 717–729, Feb. 1988, Doi: 10.1557/PROC-121-717/METRICS.

[67] A. Salmatonidis *et al.*, “Workplace Exposure to Nanoparticles during Thermal Spraying of Ceramic Coatings,” *Ann Work Expo Health*, vol. 63, no. 1, pp. 91–106, Jan. 2019, Doi: 10.1093/ANNWEH/WXY094.

[68] Y. Ding *et al.*, “Airborne engineered nanomaterials in the workplace—a review of release and worker exposure during nanomaterial production and

handling processes," *J Hazard Mater*, vol. 322, pp. 17–28, Jan. 2017, Doi: 10.1016/J.JHAZMAT.2016.04.075.

[69] S. Manna, M. K. Naskar, and S. K. Medda, "Mesoporous silica-based abrasion resistant antireflective (AR)-cum-hydrophobic coatings on textured solar cover glasses by a spray coating technique," *Mater Adv*, vol. 3, no. 7, pp. 3208–3217, Feb. 2022, Doi: 10.1039/d1ma01141c.

[70] D. B. Emrie, "Sol-Gel Synthesis of Nanostructured Mesoporous Silica Powder and Thin Films," 2024, *Hindawi Limited*. Doi: 10.1155/2024/6109770.

[71] L. P. Singh *et al.*, "Sol-Gel processing of silica nanoparticles and their applications," 2014, *Elsevier B.V.* Doi: 10.1016/j.cis.2014.10.007.

[72] S. Cai, Y. Zhang, H. Zhang, H. Yan, H. Lv, and B. Jiang, "Sol-gel preparation of hydrophobic silica antireflective coatings with low refractive index by base/acid two-step catalysis," *ACS Appl Mater Interfaces*, vol. 6, no. 14, pp. 11470–11475, Jul. 2014, Doi: 10.1021/AM501972Y.

[73] H. E. Bergna, "Downloaded via 105.232.144.30 on October 16," UTC, 2024. [Online]. Available: https://pubs.acs.org/sharingguidelines

[74] B. Xia, J. Luo, Y. Li, B. Yang, S. Zhang, and B. Jiang, "Preparation of sponge-like porous SiO2 antireflective coatings with excellent environment-resistance by an acid-catalysed sol-gel method," *RSC Adv*, vol. 7, no. 43, pp. 26834–26838, 2017, Doi: 10.1039/c7ra00622e.

[75] O. W. Flörke *et al.*, “Silica,” in *Ullmann’s Encyclopedia of Industrial Chemistry*, Wiley, 2008. Doi: 10.1002/14356007.a23_583.pub3.

[76] H. Liu, H. Kaya, Y. T. Lin, A. Ogrinc, and S. H. Kim, “Vibrational spectroscopy analysis of silica and silicate glass networks,” *Journal of the American Ceramic Society*, vol. 105, no. 4, pp. 2355–2384, Apr. 2022, Doi: 10.1111/JACE.18206.

[77] R. A. Yalçın, E. Blandre, K. Joulain, and J. Drévillon, “Daytime radiative cooling with silica fiber network,” *Solar Energy Materials and Solar Cells*, vol. 206, Mar. 2020, Doi: 10.1016/j.solmat.2019.110320.

[78] A. Aili *et al.*, “Passive daytime radiative cooling: Moving beyond materials towards real-world applications,” *Next Energy*, vol. 3, p. 100121, Apr. 2024, Doi: 10.1016/j.nxener.2024.100121.

[79] M. Lee *et al.*, “Photonic structures in radiative cooling,” *Light: Science & Applications 2023 12:1*, vol. 12, no. 1, pp. 1–29, Jun. 2023, Doi: 10.1038/s41377-023-01119-0.

[80] G. Huang *et al.*, “Radiative cooling and indoor light management enabled by a transparent and self-cleaning polymer-based metamaterial,” *Nat Commun*, vol. 15, no. 1, Dec. 2024, Doi: 10.1038/s41467-024-48150-2.

[81] J. Liu *et al.*, “Passive Photovoltaic Cooling: Advances Toward Low-Temperature Operation,” *Adv Energy Mater*, vol. 14, no. 2, Jan. 2024, Doi: 10.1002/AENM.202302662.

[82] H. Di Wang *et al.*, “Superhydrophobic porous film for daytime radiative cooling,” *Appl Mater Today*, vol. 24, Sep. 2021, Doi: 10.1016/j.apmt.2021.101100.

[83] E. Akerboom, T. Veeken, C. Hecker, J. Van De Groep, and A. Polman, “Passive Radiative Cooling of Silicon Solar Modules with Photonic Silica Microcylinders,” *ACS Photonics*, vol. 9, no. 12, pp. 3831–3840, Dec. 2022, Doi: 10.1021/acsphotonics.2c01389.

[84] H. Ye *et al.*, “Preparation of antireflective coatings with high transmittance and enhanced abrasion-resistance by a base/acid two-step catalyzed sol-gel process,” *Solar Energy Materials and Solar Cells*, vol. 95, no. 8, pp. 2347–2351, Aug. 2011, Doi: 10.1016/j.solmat.2011.04.004.

[85] V. Bueno and S. Ghoshal, “Self-Assembled Surfactant-Templated Synthesis of Porous Hollow Silica Nanoparticles: Mechanism of Formation and Feasibility of Post-Synthesis Nanoencapsulation,” *Langmuir*, vol. 36, no. 48, pp. 14633–14643, Dec. 2020, Doi: 10.1021/ACS.LANGMUIR.0C02501.

[86] C. De La Encarnacion Bermudez, E. Haddadi, E. Rampazzo, L. Petrizza, L. Prodi, and D. Genovese, “Core-Shell Pluronic-Organosilica Nanoparticles with Controlled Polarity and Oxygen Permeability,” *Langmuir*, vol. 37, no. 16, pp. 4802–4809, Apr. 2021, Doi: 10.1021/ACS.LANGMUIR.0C03531.

[87] D. R. Dunphy, P. H. Sheth, F. L. Garcia, and C. J. Brinker, “Enlarged pore size in mesoporous silica films templated by pluronic F127: Use of poloxamer mixtures and increased template/SiO2 ratios in materials synthesized by

evaporation-induced self-assembly," *Chemistry of Materials*, vol. 27, no. 1, pp. 75–84, Jan. 2015, Doi: 10.1021/cm5031624.

[88] F. Chi *et al.*, "Enhancing mechanical stability of sol-gel silica antireflection coatings via ammonia treatment at low temperature," *Results Phys*, vol. 18, p. 103315, Sep. 2020, Doi: 10.1016/J.RINP.2020.103315.

[89] W. Zhou, R. Apkarian, Z. L. Wang, and D. Joy, "Fundamentals of Scanning Electron Microscopy (SEM)," *Scanning Microscopy for Nanotechnology: Techniques and Applications*, pp. 1–40, 2006, Doi: 10.1007/978-0-387-39620-0_1.

[90] M. Abd Mutalib, M. A. Rahman, M. H. D. Othman, A. F. Ismail, and J. Jaafar, "Scanning Electron Microscopy (SEM) and Energy-Dispersive X-Ray (EDX) Spectroscopy," *Membrane Characterization*, pp. 161–179, Jan. 2017, Doi: 10.1016/B978-0-444-63776-5.00009-7.

[91] S. J. Pennycook *et al.*, "Scanning Transmission Electron Microscopy for Nanostructure Characterization," *Scanning Microscopy for Nanotechnology: Techniques and Applications*, pp. 152–191, 2006, Doi: 10.1007/978-0-387-39620-0_6.

[92] C. W. Brown, "Ultraviolet, visible, near-infrared spectrophotometers," *Analytical Instrumentation Handbook, Third Edition*, pp. 127–139, Jan. 2004, Doi: 10.1201/9781315118024-5.

[93] M. A. Mohamed, J. Jaafar, A. F. Ismail, M. H. D. Othman, and M. A. Rahman, "Fourier Transform Infrared (FTIR) Spectroscopy," *Membrane*

Characterization, pp. 3–29, Jan. 2017, Doi: 10.1016/B978-0-444-63776-5.00001-2.

[94] D. P. Subedi, D. K. Madhup, A. Sharma, U. M. Joshi, and A. Huczko, "Retracted: Study of the wettability of ZnO nanofilms," *Int Nano Lett*, vol. 2, no. 1, Dec. 2012, Doi: 10.1186/2228-5326-2-1.

[95] M. Cullen, A. Kaworek, J. Mohan, B. Duffy, and M. Oubaha, "An investigation into the Role of the Acid Catalyst on the Structure and Anticorrosion Properties of Hybrid Sol-Gel Coatings," *Thin Solid Films*, vol. 729, p. 138703, Jul. 2021, Doi: 10.1016/J.TSF.2021.138703.

[96] P. Fu, G. Le Teri, X. L. Chao, J. Li, Y. H. Li, and H. Yang, "Modified graphene-feve composite coatings: Application in the repair of ancient architectural color paintings," *Coatings*, vol. 10, no. 12, pp. 1–12, Dec. 2020, Doi: 10.3390/coatings10121162.

[97] Z. Han, J. Yuan, P. Tian, B. Liu, J. Tan, and Q. Zhang, "Preparation of highly transparent and wear-resistant SiO2 coating by alkali/acid dual catalysed sol–gel method," *J Mater Res*, vol. 38, no. 13, pp. 3316–3323, Jul. 2023, Doi: 10.1557/S43578-023-01062-1.

[98] W. Wei, X. Zhu, Y. Zhao, and Q. Wu, "Nanometer SiO_2Antireflection Coating for Solar Modules," pp. 36–39, Mar. 2016, Doi: 10.2991/MEEP-15.2016.10.

[99] H. Zou, S. Wu, and J. Shen, "Polymer/Silica Nanocomposites: Preparation, characterization, properties, and applications," Sep. 2008. Doi: 10.1021/cr068035q.

[100] Y. Y. Huang and K. Sen Chou, “Studies on the spin coating process of silica films,” *Ceram Int*, vol. 29, no. 5, pp. 485–493, 2003, Doi: 10.1016/S0272-8842(02)00191-8.

[101] C. A. Milea, C. Bogatu, and A. Duta, “The Influence of Parameters in Silica Sol- Gel Process,” *Bulletin of the Transilvania University of Brasov. Series I - Engineering Sciences*, pp. 59–66, Jul. 2011, Accessed: Nov. 04, 2024. [Online]. Available: https://webbut.unitbv.ro/index.php/Series_I/article/view/6140

[102] R. Ciriminna, A. Fidalgo, V. Pandarus, F. Béland, L. M. Ilharco, and M. Pagliaro, “The sol-gel route to advanced silica-based materials and recent applications,” *Chem Rev*, vol. 113, no. 8, pp. 6592–6620, Aug. 2013, Doi: 10.1021/CR300399C/ASSET.

[103] S. Dervin and S. C. Pillai, “An Introduction to Sol-Gel Processing for Aerogels,” pp. 1–22, 2017, Doi: 10.1007/978-3-319-50144-4_1.

[104] C. J. Brinker and G. W. Scherer, “Sol → gel → glass: I. Gelation and gel structure,” *J Non Cryst Solids*, vol. 70, no. 3, pp. 301–322, Apr. 1985, Doi: 10.1016/0022-3093(85)90103-6.

[105] H. K. Raut, A. S. Nair, S. S. Dinachali, V. A. Ganesh, T. M. Walsh, and S. Ramakrishna, “Porous SiO2 anti-reflective coatings on large-area substrates by electrospinning and their application to solar modules,” *Solar Energy Materials and Solar Cells*, vol. 111, pp. 9–15, 2013, Doi: 10.1016/j.solmat.2012.12.023.

[106] X. Li *et al.*, “Fabrication of single-layer antireflective coating with environmental stability by modified SiO_2 mixed sol,” *Colloids Surf A Physicochem Eng Asp*, vol. 630, Dec. 2021, Doi: 10.1016/J.COLSURFA.2021.127553.

[107] K. Y. Law, “Definitions for hydrophilicity, hydrophobicity, and superhydrophobicity: Getting the basics right,” *Journal of Physical Chemistry Letters*, vol. 5, no. 4, pp. 686–688, Feb. 2014, Doi: 10.1021/JZ402762H.

[108] B. J. Basu, V. Hariprakash, S. T. Aruna, R. V. Lakshmi, J. Manasa, and B. S. Shruthi, “Effect of microstructure and surface roughness on the wettability of superhydrophobic Sol-gel nanocomposite coatings,” *J Solgel Sci Technol*, vol. 56, no. 3, pp. 278–286, Dec. 2010, Doi: 10.1007/S10971-010-2304-8.

Appendices

Appendix A

UNAM
UNIVERSITY OF NAMIBIA

ETHICAL CLEARANCE CERTIFICATE

Ethical Clearance Reference Number: SOS-0232 **Date: 23AUGUST 2024**

This Ethical Clearance Certificate is issued by the University of Namibia Ethics Committee (REC) in accordance with the University of Namibia's Research Ethics Policy and Guidelines. Ethical approval is given in respect of undertakings contained in the Research Project outlined below. This Certificate is issued on the recommendations of the ethical evaluation done by the ethics committee.

Title of Project:	ENHANCING SOLAR PHOTOVOLTAIC EFFICIENCY WITH POROUS SILICA COATINGS
Student:	LEONARD ETUNA NAMWIHA
Student Number:	222177225
Supervisor(s):	DR. PETJA DOBREVA PROF. BRYCE RICHARDS

Centre for Research Services

Take note of the following:

1. Any significant changes in the conditions or undertakings outlined in the approved Proposal must be communicated to the ethics committee. An application to make amendments may be necessary.
2. Any breaches of ethical undertakings or practices that have an impact on ethical conduct of the research must be reported to the ethics committee.
3. The Principal Researcher must report issues of ethical compliance to the ethics committee (through the Chairperson) at the end of the Project or as may be requested by the ethics committee.
4. The ethics committee retains the right to:

i) Withdraw or amend this Ethical Clearance if any unethical practices (as outlined in the Research Ethics Policy) have been detected or suspected,

ii) Request for an ethical compliance report at any point during the course of the research.

The ethics committee wishes you the best in your research.

Prof. Ezekeil Gwinyai Kwembeya (Chairperson Ethics Committee)

Prof. Davis Mumbengegwi (Head, Multidisciplinary Research)

Appendix B

CENTRE FOR RESEARCH SERVICES
Office of the Pro-Vice Chancellor: Research, Innovation & Development
University of Namibia, Private Bag 13301, Windhoek, Namibia
340 Mandume Ndemufayo Avenue, Pioneers Park, Office F223 - Florck, Second Floor
☎ +264 61 206 4673; E-mail:kmbulu@unam.na; URL: http://www.unam.edu.na

UNAM
UNIVERSITY OF NAMIBIA

RESEARCH PERMISSION LETTER

Date: 28/10/2024

Student Name: LEONARD ETUNA NAMWIHA

Student Number: 222177225

Programme: Master of Science in Renewable Energy

Approved Research Title: ENHANCING SOLAR PHOTOVOLTAIC EFFICIENCY WITH POROUS SILICA COATINGS

TO WHOM IT MAY CONCERN:

I hereby confirm that the above-mentioned student is registered at the University of Namibia for the programme indicated. The proposed study met all the requirements as stipulated in the University guidelines and has been approved by the relevant committees.

The proposal adheres to ethical principles as per attached Ethical Clearance Certificate. Permission is hereby granted to carry out the research as described in the approved proposal.

Best Regards

Dr. AEE Shikongo
Head: Postgraduate Research Support Services
Tel: +264 61 206 3129
E-mail: aeshikongo@unam.na

CENTRE FOR RESEARCH SERVICES
Office of the Director
2024 -10- 28
University of Namibia
UNAM

Appendix C

Karlsruher Institut für Technologie

KIT-Campus North | IMT | P.O. Box 3640 | 76021 Karlsruhe, Germany

Mr. Leonard Etuna Namwiha
136 R Ruzo Street,
Windhoek,
Namibia
Tel: +264 81 3113636
Email: leonardnamwiha@gmail.com

Prof. Dr. Bryce S. Richards

Professor of Nanophotonics for Energy
Co-Director of IMT and LTI

Institute of Microstructure Technology (IMT)
Hermann-von-Helmholtz-Platz 1
76344 Eggenstein-Leopoldshafen, Germany
Phone: +49 721 608-26562
Web: www.imt.kit.edu

Light Technology Institute (LTI)
Engesserstrasse 13
76131 Karlsruhe, Germany
Phone: +49 721 608-41998
Web: www.lti.kit.edu

Email: bryce.richards@kit.edu

Pages: 1

16th February 2024

Invitation letter for Mr. Leonard Etuna Namwiha to conduct his Masters thesis project at KIT

To whom it may concern,

I would like to invite Mr. Leonard Etuna Namwiha (born on 06.09.1995 in Namibia) to conduct a research stay within the Institute for Microstructure Technology (IMT) at the Karlsruhe Institute of Technology (KIT).

Mr. Namwiha is enrolled as a Masters student at the University of Namibia (UNAM), where I am in close contact with his local supervisor, Dr. Petja Dobreva. Mr. Namwhia will come to KIT to carry out a 6-month research project for his Masters degree. This will be conducted under the supervision of Dr. Gan Huang and myself. The research project begins on 1st April 2024 is entitled "*Enhancing Photovoltaic Efficiency with Optical Coatings*". It should be noted that this is a research stay only and during his time at KIT, Mr. Namwiha will not attend lectures or write exams.

We would all be grateful if his visa could be issued promptly so that there is no adverse impact on his studies.

Please do not hesitate to contact me via phone or email if you require more information.

Thank you!

Best regards

Prof. Dr Bryce S. Richards

Co-Director IMT / KIT